Optical Materials 92 (2019) 111–124

Contents lists available at ScienceDirect

Optical Materials

journal homepage: www.elsevier.com/locate/optmat

# Experimental and theoretical studies on the bifurcated hydrogen bonded NLO active material of pure and crystal violet dye-doped L-argininium bis dihydrogen phosphate

Reena Ittyachan[a,*], Jesby George[b], Ligi Cherian[c], Lynnette Joseph[b], D. Sajan[b,**], G. Vinitha[d]

[a] Department of Physics, Sacred Heart College, Chalakudy, Kerala, 680307, India
[b] Centre for Advanced Functional Materials, Department of Physics, Bishop Moore College, Mavelikara, Alappuzha, Kerala, 690110, India
[c] Department of Physics, Christian College, Chengannur, 689 122, Kerala, India
[d] Division of Physics, School of Advanced Sciences, Vellore Institute of Technology (VIT), Chennai, 600127, India

ARTICLE INFO

*Keywords:*
Crystal growth
Bifurcated H-Bonds
Blue and red shifting H-Bonds
Hole-electron transport
NLO
Z-scan

ABSTRACT

Single crystals of pure and crystal violet dye-doped L-Argininium bis dihydrogen phosphate were grown using slow evaporation technique. The crystalline nature and the structure parameters were confirmed by powder X-ray diffraction technique. Blue and red shifting hydrogen bonds were predicted by DFT on the basis of vibrational spectral (FT-IR & FT-Raman), AIM and NBO analyses. Bifurcated N—H···O and O—H···O intermolecular hydrogen bonds in LADP molecule were visualized by Hirshfeld surface. $^{13}C$ and $^{1}H$ NMR spectroscopy confirmed the structure of LADP. Doped LADP crystal shows enhancements in the wavelength and longer lifetimes as identified from photoluminescence spectra and decay analysis respectively. The high values of electron mobility and low value of $\lambda_{electron}$ reflect the applicability of LADP in OLED devices. Enhancement in nonlinear optical parameters in dye-doped LADP crystal was revealed from the Z-scan technique which shows its usefulness in the fabrication of NLO devices.

## 1. Introduction

L-Arginine derivatives are good NLO materials due to their zwitterionic form which they acquire from the protonation of guanidyl and alpha-amino groups as well as from the deprotonation of a carboxyl group to either organic or inorganic salts, through inter and intramolecular interactions [1–3]. Studies on organic and inorganic complexes based on acid-base interactions showing high optical nonlinearity, mechanical strength and thermal stability [4], points out that in such systems highly polarizable cations responsible for NLO properties are conjugated to inorganic anions through intermolecular hydrogen bonding which generates a non-centrosymmetric crystal structure. Bifurcated hydrogen bonds have been proved to be responsible for the stability in the supramolecular architectures [5,6] and the charge transfer from the organic part into the inorganic part leads to high nonlinear response [7]. The network of hydrogen bonds in a single molecule contribute to its large values of hyperpolarizability and charge transfer interactions which make it useful in nonlinear optical applications like frequency conversion, optical modulation and optical switching [8–10]. The rigorous research pursued on the L-arginine -phosphate crystals in both pure and doped forms shows its excellent nonlinear optical properties [10–12] owing to its wide transparency range, dipolar strength and chemical as well as thermal stability [13,14]. Due to increasing applications in optoelectronic device fabrication, researchers are attracted in the inclusion of dye in crystals [15–18]. The crystal violet (triphenylmethane) dye alters the molecular structures and has received more attention in both fundamental and applied physical chemistry [21,22]. The chemical synthesis of crystals by the addition of a dye produces intermolecular interactions which enhance their luminescence efficiency [19,20]. The present study reports the synthesis of crystal violet doped L-argininium bis dihydrogen Phosphate (CVLADP) and an investigation of its photophysical, thermal and structural NLO properties using Density functional theory (DFT) and experimental spectral characterizations.

* Corresponding author.
** Corresponding author.
*E-mail addresses:* reenaittyachan@gmail.com (R. Ittyachan), drsajanbmc@gmail.com, dsajanbmc@gmail.com (D. Sajan).

https://doi.org/10.1016/j.optmat.2019.04.019
Received 16 November 2018; Received in revised form 6 April 2019; Accepted 8 April 2019

## 2. Methods

### 2.1. Experimental methods

#### 2.1.1. Crystal growth

Crystals of LADP were grown from aqueous solution by slow evaporation technique. High purity L-arginine [Kemphasol 98%] and orthophosphoric acid in the stoichiometric ratio 1:2 were mixed in millipore water to prepare the solution of LADP. Those crystals were grinded well to make LADP powder. A saturated solution was prepared using LADP powder and distilled water. The prepared solution was filtered and then adds 0.7 mole CV dye was added to it. From the saturated solution of dye-doped LADP, a small amount was poured into a petri dish and covered with a glass paper with small holes in it. After 3 weeks small violet colored crystals are obtained. From these, crystals with perfect morphology and those free from macro defect were selected as seed crystals.

A seed crystal of minimum size was immersed in the saturated solution of dye-doped LADP by using a nail and thread arrangement and covered it with glass paper with a small hole in it. The growth of the crystal was observed daily. Good quality large crystal of crystal violet dye-doped LADP was grown after 50 days. Crystal was grown up to $55 \times 8 \times 5\,mm^3$. The obtained seed crystal and grown crystals are shown in Fig. 1.

#### 2.1.2. Instrumentation details

The grown crystals were subjected to Powder X-ray diffraction using the Rigaku MinFlex 600, tabletop XRD diffractometer operated at 40 kV and 15 mA with monochromated Cu Ka radiation (λ = 1.5406 Å). $^1H$ NMR and $^{13}C$ NMR spectral analyses were carried out for the samples in water solvent using Bruker 400 MHz NMR spectrometer. FT-IR spectra of the sample were recorded using the Perkin Elmer Spectrum Two: FT-IR spectrometer in the scan range 4000–450 $cm^{-1}$ with a resolution of 1 $cm^{-1}$. FT-Raman spectrum was recorded using a BRUKER RFS27 FT-Raman spectrometer. UV–Vis–NIR absorption spectral data of the sample in water solution were obtained using JASCO V-760 Spectrophotometer in the region 187–800 nm. The photoluminescence (PL) measurement was made on pure and doped samples using a Jobin Yvon-Spex Spectrofluorometer with 450 W high-pressure xenon lamp as an excitation source.

The Z-scan measurement of the sample was carried out using a 50 mW, 532 nm diode-pumped Nd: YAG laser beam which was focused by a lens with 3.5 cm focal length. A 1 mm wide optical cell containing the solution of the sample with around 63% transmittance was translated across the focal region along the axial direction (z-direction). The intensity of the focused laser beam transmitted through the sample was measured with the help of a digital power meter. The experimental set-up for the demonstration of optical limiting under CW illumination is very similar to the Z-scan geometry [34,35].

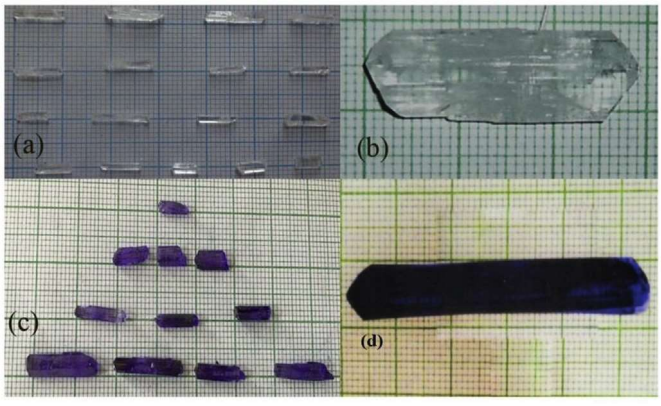


**Fig. 1.** (a) Seed crystals of LADP (b) grown LADP crystal (c) seed crystals of CV dye-doped LADP (d) Grown CV doped LADP crystal.

### 2.2. Computational details

Quantum chemical calculation was performed using the Gaussian 09 [23,24] program package supplemented with the standard B3LYP/6-31 + + G (d,p) basis set for an isolated molecule. Detailed vibrational assignments for the theoretical vibrational spectra for LADP were carried out by potential energy distribution (PED) analysis using MOLVIB 7.0 program [25,26] with scaled quantum mechanical force field (SQMFF) method and was compared with experimental FT-IR and FT-Raman spectra. Natural Bond Orbital (NBO) analyses were performed to investigate the intermolecular bonding and interaction [27]. The electron densities at the bond critical points (BCP) were analyzed using the atoms in molecules (AIM) approach using the AIMALL package [28]. The dipole moment, mean polarizability and dynamic first and second hyperpolarizabilities were calculated at the 532 nm ($\hbar\omega = 0.0857a.u$) laser wavelength. The details used for the calculation of dipole moment, polarizability, first order hyperpolarizabilities viz. β(-2ω; ω, ω) and β(-ω; ω, 0), second-order hyperpolarizability for quadratic electro-optic Kerr effect, γ(-ω; ω, 0, 0), and the DC electric field induced, γ(-2ω; ω, ω, 0), are reported in literature [29,30].

## 3. Results and discussion

### 3.1. Powder X-ray diffraction (PXRD) analysis

The comparison between the PXRD patterns of grown crystals of pure and dye-doped LADP with the simulated single crystal XRD [31] spectral patterns are shown in Fig. 2. The PXRD pattern revealed that

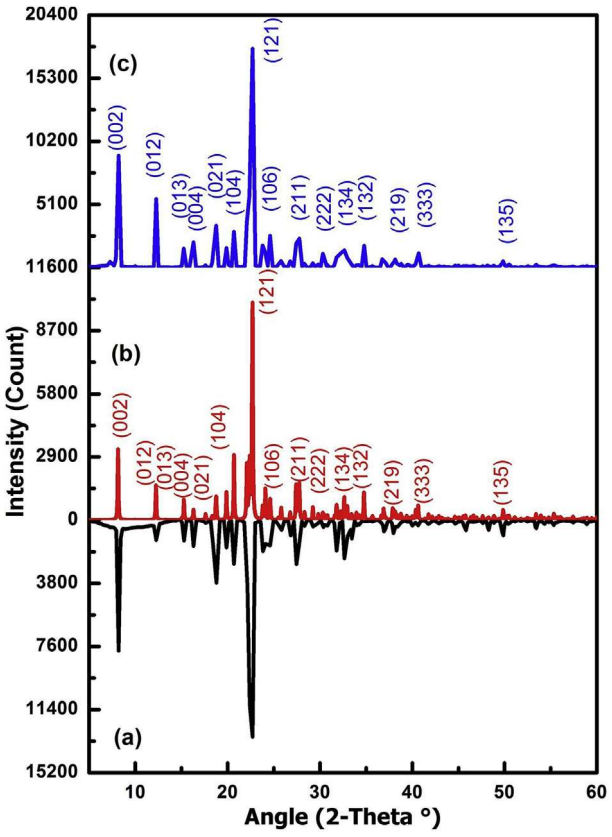


**Fig. 2.** (a) experimental PXRD pattern of pure LADP crystal (b) simulated PXRD pattern from SXRD data [31] of pure LADP generated by Mercury 3.0 program (c) experimental PXRD pattern of doped LADP crystal.

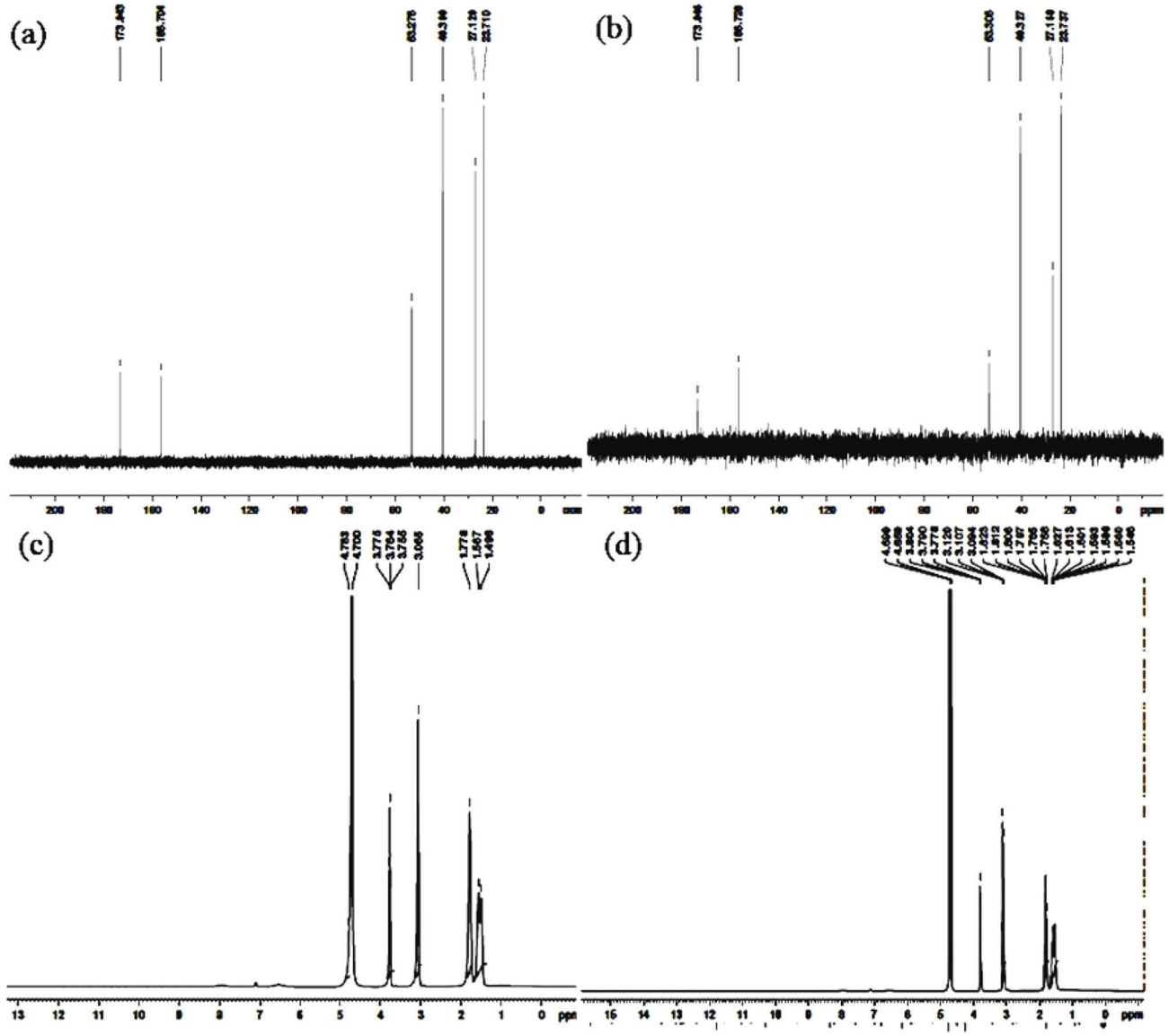


**Fig. 3.** (a) & (b) are $^{13}C$ NMR spectra of pure LADP and CV doped LADP in water (c) & (d) $^{1}H$ NMR spectra of pure LADP and CV doped LADP in water.

exact identities of the grown pure and dye-doped LADP crystallize in the orthorhombic system with non-centrosymmetric $P2_12_12_1$ space groups. The lattice parameters were evaluated as a = 7.0692 Å, b = 9.6321 Å, c = 21.7281 Å, $\alpha = \beta = \gamma = 90^0$ for LADP and a = 7.0663 Å, b = 9.6388 Å, c = 21.74636 Å, $\alpha = \beta = \gamma = 90^0$ for dye-doped LADP. The calculated cell parameters obtained from the PXRD are in good agreement with the reported values [31]. The substitutional or interstitial addition of CV dopant shows a slight change in the unit cell parameters of CVLADP.

### 3.2. NMR spectral analysis

The $^{13}C$ and $^{1}H$ NMR theoretical calculations were done in water solvent phase using the basis set GIAO-B3LYP/6-31 + + G (d,p), which provides the effect of nuclear shielding in LADP molecule. The theoretical calculations, as well as the experimental values of LADP, are shown in the Table TS1 (Supplementary Information). The experimental $^{13}C$ and $^{1}H$ NMR spectra using $D_2O$ solvent in the pure and doped LADP crystals are shown in Fig. 3 The absence of proton signals of $NH_3^+$-amino and guanidyl group of the L-arginine cations in the $^{1}H$ NMR spectrum is due to the replacement of the protons by deuterium atoms. The intense signal at 4.700 ppm manifests the residual shift of $H_2O$ solution. The CH proton shows its signal at 3.775 ppm. The aliphatic $CH_2$ protons signals at 3.065, 1.778 and 1.498 ppm are assigned to $C_{25}$, $C_{24}$ and $C_{23}$ protons respectively. The OH protons of dihydrogen phosphate anion shows signals at 3.764, 3.775 and 4.783 ppm are assigned to $O_{11}$, $O_9$ , and $O_7$ respectively. The proton chemical shift of doped LADP in Fig. 3(d) are similar to that of pure LADP.

Chemical shift of $^{13}C$ NMR spectrums of pure and doped LADP crystals in water solution are shown in Fig. 3(a) and (b) respectively. The $^{13}C$ NMR spectrum exhibits six signals with respect to six carbon atoms of different chemical environments. From the spectrum, the signal at 53.267 ppm is due to the presence of CH group in the L-arginine cation. The signals at 27.12, 23.71 and 40.3 ppm are attributed to the presence $CH_2$ carbons of $C_{23}$, $C_{24,}$ and $C_{25}$ respectively for the L-arginine cations. An intense signal was observed at 156.704 ppm due to the presence of carbon $C_{26}$ atom in the guanidyl group. The signal at 173.043 ppm is due to the presence of carbonyl carbon $C_{21}$of COOH group in the L-arginine cation. The $^{13}C$ NMR spectra in Fig. 3(b) shows that the signals from doped LADP are similar to that of the pure LADP.

### 3.3. Thermal analysis

The thermal stability of pure and doped LADP crystals was

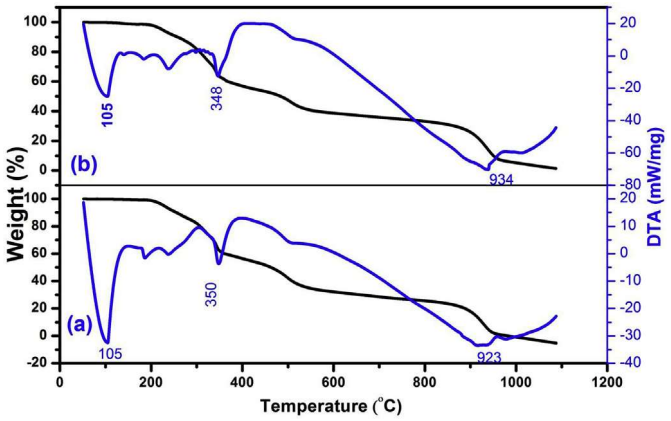


**Fig. 4.** Thermogravimetric analysis spectrum of (a) doped (b) pure LADP crystals.

examined by thermogravimetric (TG) and differential thermal analysis (DTA). The samples of pure LADP (weight-5.44 mg) and the crystal violet doped LADP (weight-2.37 mg) was analyzed by UniversalV4.5A TA Instruments between the temperature range 50 °C and 1100 °C in the nitrogen atmosphere with heating rate 20 °C/min as shown in Fig. 4. The DTA trace shows a sharp endothermic peak at around 100 °C which is attributed to the melting point of LADP. The TG curve shows two stages of significant weight loss pattern. Major weight loss started from 216 °C to 900 °C with the mass change of 75% and 82% in pure and doped LADP respectively, which is assigned to the complete decomposition of L-arginine cation [32]. The increasing weight loss percentage in the doped LADP samples reveals the incorporation of crystal violet dopant in the crystal lattice of LADP. The second stage of weight loss starts from above 900 °C, which is due to the elimination of phosphate anions [32].

### 3.4. UV–vis analysis

Optical absorption range and absorption peak position are important for NLO active compounds [71]. Fig. 5(a) shows that the absorption edge of the doped LADP crystals is shifted to the lower wavelength values. It is observed that the absorption edge present at 202 and 192 nm in pure and doped LADP crystals respectively, corresponds to strong n→π* transition associated with intermolecular hydrogen bonding [70]. The band gap of doped sample is greater compared to that of pure LADP, which lead to a blue shift as shown in Fig. 5 (b). The doped crystal has increased transparency which indicates its potential to be used as an excellent optical material [33].

### 3.5. Photoluminescence studies

The photoluminescence (PL) spectrum of LADP is due to the electron acceptor group of N—H sites of the cations and electron withdrawing group of O—H sites in the hydrogen phosphate anion groups. The emission spectrum in Fig. 6(a) was carried out in the wavelength range 340–600 nm with the excitation wavelength 320 nm on pure and CV doped LADP crystals at the water solvent. The pure and doped samples show blue emission property which was inferred from the presence of broad emission bands centered at 403 and 414 nm respectively. This blue shifting of the PL spectrum of crystal violet doped LADP is attributed to the inclusion of dye atoms in the interstitials cites of LADP. Moreover, due to the dye doping, the effective band gap increases which result in comparatively high energy values for the emitted photons. Hence, these high energy photons give photoluminescence peaks at a shorter wavelength as evident from the PL spectra. The decreased luminescence broadness of dye-doped crystals indicates the usefulness of these crystals for developing coherent sources in applications that require blue light. The PL spectrum revealed that CV dye doping increases the fluorescence efficiency and the sharpness of the emission band in LADP [4].

The fluorescence decay curve of the pure and doped LADP crystals at 403 and 413 nm respectively under the excitation of 330 nm laser light is shown in Fig. 6 (b). The fluorescence lifetime curves were fitted with third exponential decay functions. The average fluorescence lifetime is found to be 2.95 ns and 8.49 ns for pure and CVLADP respectively. The fluorescence decay time was increased by CV doping. The decay component of lifetime and amplitude from the present study is presented in Table 1. The quality of the curve fit was calculated by the value of the reduced $\chi^2$ ratio; appropriate value for CVLADP than pure LADP. The fluorescence lifetime results of the CVLADP gives blue emission for a significant lifetime than the pure LADP for blue light emitting devices.

The colour of the phosphorescence is calculated from the emission

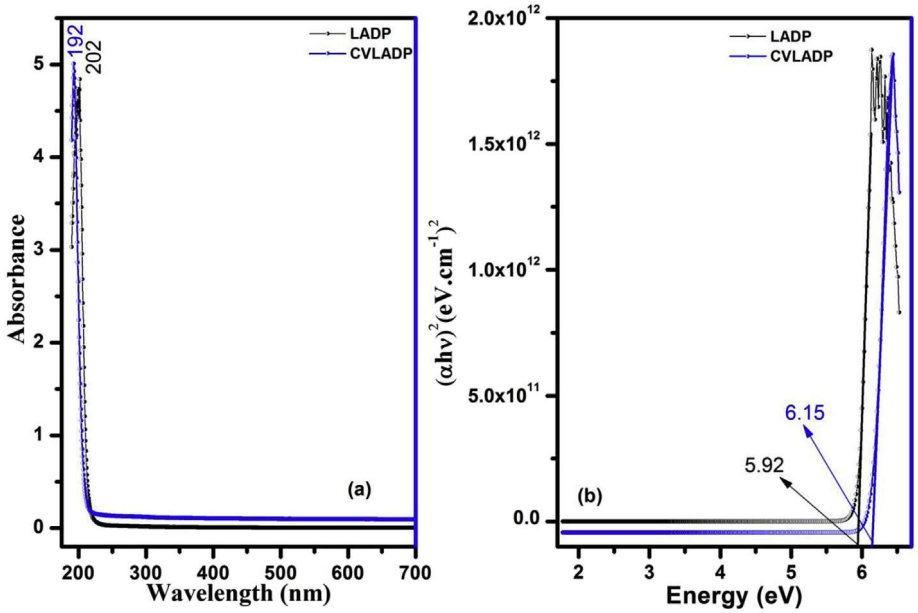


**Fig. 5.** (a) UV–vis–NIR absorbance plots of the pure and doped crystals in water solution(b) the tauc plot for pure and doped LADP.

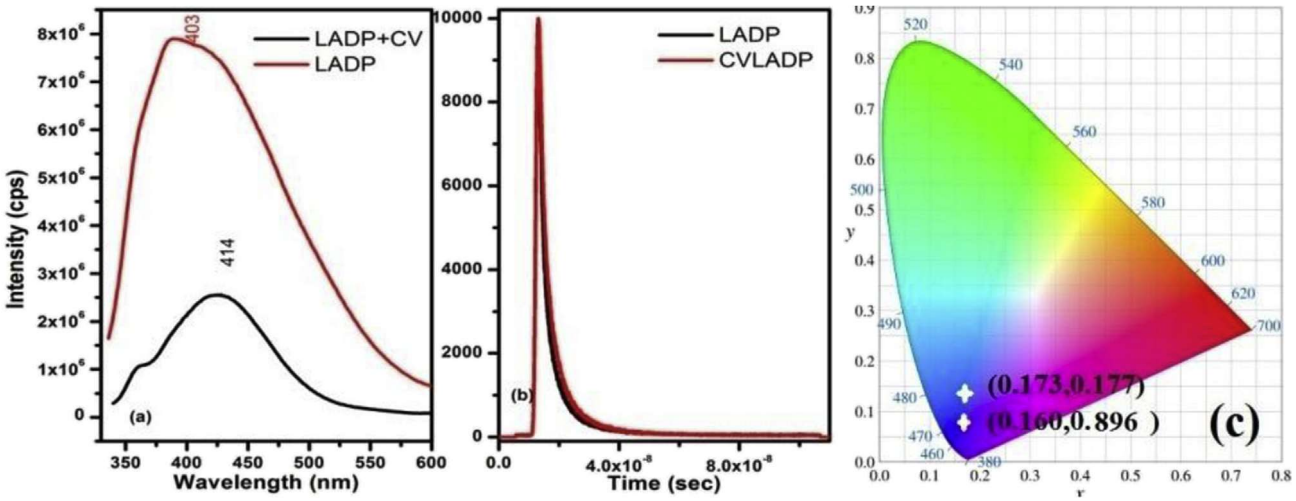


**Fig. 6.** (a) PL spectra of the grown pure and doped LADP crystal. (b) Luminescence decay of the pure doped LADP at 330 nm (c) CIE Chromaticity diagram of pure and doped LADP crystal.

spectrum using the chromaticity coordinate based on the CIE 1931 (Commission International d'Eclairage) system. The chromaticity coordinates of the pure and CVLADP crystals are (0.173, 0.177) and (0.160, 0.0896) respectively, which indicate the light emission in the blue region of visible region of electromagnetic radiation. Low values of CIE coordinates illustrate the decrease in the fluorescence intensity of CVLADP. From CIE chromaticity diagram Fig. 6(c), it is clear that the colour is located in the blue region.

### 3.6. Z-scan studies

Third-order nonlinear optical quantities such as nonlinear refractive index ($n_2$),the nonlinear absorption coefficient (β) and nonlinear susceptibilities ($\chi^{(3)}$) have been investigated through the Z-scan technique developed by Sheik-Bahae et al. [34,35]. Nonlinear absorption and nonlinear refraction was detected by placing an aperture in front of the detector which is called closed-aperture Z-scan, whereas, pure nonlinear absorption was detected by the absence of aperture which is called open aperture Z-scan. The ratio of closed to open is taken in order to obtain pure nonlinear refraction. The values of $n_2$, $\chi^{(3)}$, β and second hyperpolarizability (γ) were calculated using standard relations [36,37]. Fig. 7(a) shows the closed aperture pattern of LADP and CVLADP in which peak precedes the valley indicating a negative nonlinearity arising due to self-defocusing effect. The samples were focused by the beam of continuous laser which induced thermal nonlinearity, to the spatial distribution of temperature resulting in a distortion in the propagating beam. The sample CVLADP shows higher peak-valley difference transmittance. Fig. 7(b) shows the open-aperture pattern of LADP and CVLADP which reveals the presence of saturable absorption. i.e. the absorption of light decreases with increase in the incident light intensity [38]. The nonlinear absorption coefficient (β), increases in crystal violet dopant due to the enhancement of thermal agitation resulting from the dopant. The calculated NLO coefficients of the samples are summarized in Table 2. The doped and pure LADP samples exhibit strong nonlinear refraction as compared to nonlinear absorption are reported in the literature [40–44]. This is evident from the fact that the real part of third-order nonlinear susceptibility is greater than the imaginary part of the third order nonlinear susceptibility. The crystal violet doped LADP possesses the advantages of both crystal violet and LADP leading to enhanced third order nonlinearity. The LADP crystal shows optical nonlinearities due to the donor-acceptor intermolecular interactions through bifurcated hydrogen bonds [39]. The electron delocalization and intermolecular charge transfer make the LADP compound to possess large molecular hyperpolarizability and thus contribute to large third-order susceptibility ($\chi^{(3)}$) [35].

#### 3.6.1. Optical limiting study

Optical limiters are devices that provide linear transmission below a threshold input power and hold a saturated value above the threshold input power [38]. The optical limiting behavior of the samples was tested by using a photodetector which measures the output power values with respect to their input laser power. Fig. 7 (d) shows that limiting amplitude decrease with the addition of crystal violet dopant in LADP crystal. This confirms that the limiting efficiency of LADP crystals increases with the addition of crystal violet dopant. The limiting threshold was found to be 4.4 and 4.00 mW for LADP and CVLADP samples respectively.

### 3.7. Theoretical NLO studies

The enhancement of NLO parameters such as dipole moment (μ), polarizability (α) and first and second hyperpolarizabilities (β and γ) values of the LADP crystal are due to the hydrogen bonded interactions namely $N_{17}$—$H_{34}$···$O_{12}$ (2.7548 Å), $N_{17}$—$H_{35}$ ….$O_4$ (2.7577 Å), $O_3$—$H_6$ ….$O_{12}$ (2.6286 Å) and $N_{20}$—$H_{40}$ ….$O_9$ (2.9375 Å) and $N_{18}$—$H_{37}$ ….$O_9$ (2.9226 Å) within the molecular system [45–48]. Molecular structures containing O—H ….O and N—H···O intermolecular hydrogen bond interactions generally shows an enhancement in their molecular hyperpolarizability and optical properties [56]. The first-order hyperpolarizabilities for the static $\beta(0; 0,0)$, the electro-optical Pockels effect $\beta(-\omega; \omega, \omega)$ and the second harmonic generation $\beta(-2\omega; \omega, \omega)$ for LADP were calculated to be $2.00 \times 10^{-30}$ esu, $112.270 \times 10^{-30}$ esu and $17.263 \times 10^{-30}$ esu respectively. The static second-hyperpolarizability $\gamma(0; 0,0,0)$, the frequency dependent second-hyperpolarizability

**Table 1**
Fluorescence lifetime analysis data of pure and doped LADP crystals.

| Single Crystal | Analysis | Lifetime (ns) | | | Amplitude | | | $\chi^2$ |
|---|---|---|---|---|---|---|---|---|
| | | $\tau_1$ | $\tau_2$ | $\tau_3$ | $A_1$ | $A_2$ | $A_3$ | |
| LADP | Three exponentials | 3.4883 | 1.1583 | 0.57194 | 48.22 | 27.63 | 24.15 | 1.1742 |
| CVLADP | | 3.7754 | 11.445 | 0.7661 | 52.40 | 30.61 | 16.99 | 1.1353 |

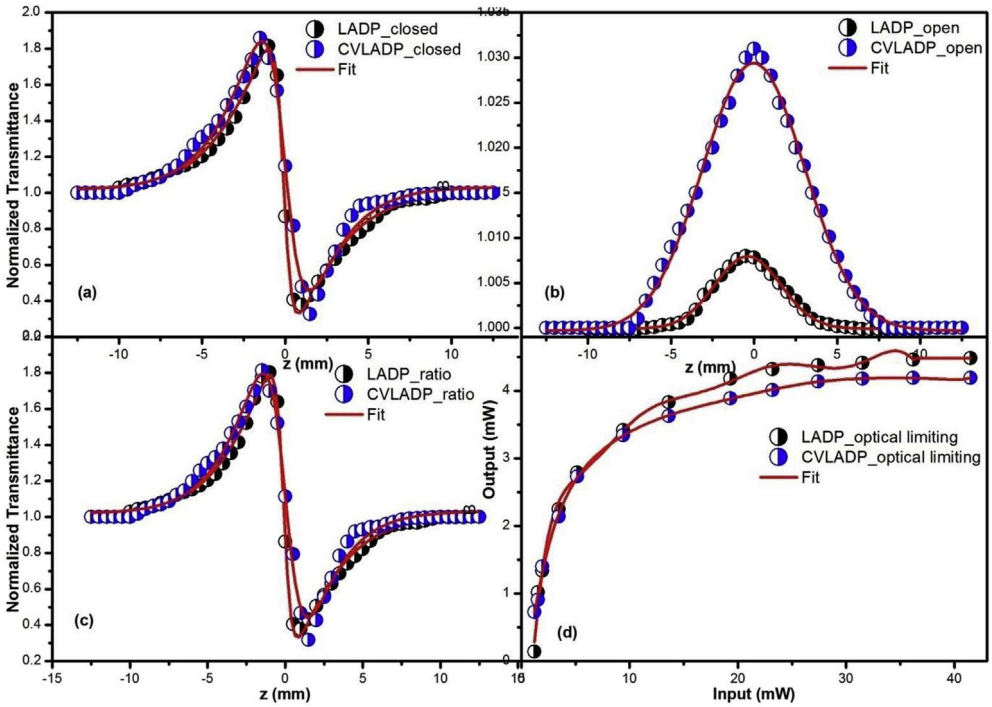


**Fig. 7.** (a) Closed aperture (b) Open aperture (c) ratio of closed to open aperture z-scan (d) Optical limiting curve for pure and doped LADP crystals.

for the quadratic electro-optic Kerr effect $\gamma(-\omega; \omega, 0,0)$ and the electric-field-induced second harmonic generation $\gamma(-2\omega; \omega, \omega, 0)$ for LADP molecule are $15.851 \times 10^{-36}$ esu, $1508.64 \times 10^{-36}$ esu and $19.825 \times 10^{-36}$ esu respectively. The obtained values for LADP and their pristine molecules are shown in Table 3 which reveals the field dependent polarizability nature of the LADP molecule.

The red and green colour regions in the highest molecular orbitals (HOMO) and lowest unoccupied molecular orbitals (LUMO) represents positive and negative phases respectively. In LADP molecule, the HOMO is located in guanidyl part of the L-argininium cation, whereas LUMO is located in the carboxylic acid and $NH_3^+$ groups in the L-argininium molecule as shown in Fig. 8. It is clear that intermolecular hydrogen bonds play an important role in the charge transfer mechanism in LADP molecule because dihydrogen phosphate anion doesn't show any active sites. The theoretically calculated HOMO-LUMO gap is 6.27 eV, which shows the semiconducting nature of LADP [73].

### 3.8. Optimized geometry

The optimized molecular structure of LADP forms through the proton transfer from O—H sites of two orthophosphoric acid molecules to the guanidyl nitrogen atom and $NH_2$ groups in the L-argininium cation. LADP molecule have L-argininium cation and two hydrogen phosphate anion contact through $N_{17}$—$H_{34}$ ….$O_{12}$, $N_{17}$—$H_{35}$ ….$O_4$, $N_{18}$—$H_{37}$ ….$O_9$ and $N_{20}$—$H_{40}$…$O_9$ intermolecular hydrogen bonds and $O_3$—$H_6$ ….$O_{12}$ intermolecular hydrogen bonds between the two dihydrogen phosphate molecules as shown in Fig. 9(a). Table TS2(Supplementary Information) shows the optimized geometric parameters obtained by B3LYP/6-31 + + G (d,p) basis set and X-ray diffraction data [17] of LADP. The strengthening of the bonds of the proton donors in the amine group are identified with the bond distance 0.890 for $N_{17}$—$H_{34}$, 0.890 for $N_{17}$—$H_{35}$ and 0.891 Å for $N_{17}$—$H_{36}$ in the XRD data. The intermolecular contacts are within the Van der Waals radii as shown in Table 4 which indicates the strength of the hydrogen bond. The oxygen atoms $O_4$ and $O_{12}$ are bifurcated hydrogen bonds and manifests formation of nine atoms ring with the $NH_3^+$ group as shown in Fig. 9(b). The oxygen atom $O_9$ act as a bifurcated hydrogen bond acceptor to the N—H bonds in the guanidyl part of the L-argininium molecule. The lengthening of N—H bonds such as $N_{17}$—$H_{34}$ (1.053 Å), $N_{17}$—$H_{35}$ (1.049), $N_{18}$—$H_{37}$ (1.021 Å) and $N_{20}$—$H_{40}$ (1.020 Å) are due to the intermolecular N—H…O interactions. The strengthening of $NH_2^+$ bond with $N_{20}$—$H_{41}$ distance, 0.859 Å, as compared to the$N_{20}$-$H_{40}$ distance, 0.860 Å, is due to the protonation of the gunidyl group. DFT also predicts strong $O_3$—$H_6$ ….$O_{12}$ hydrogen bonding interaction between the dihydrogen phosphate anions for the molecule. For a detailed understanding of the nature of the local bonding situation, we have performed DFT calculations on the gas phase molecules of L-arginine and ortho-phosphoric acid with the same basis set as described above and compared the results with LADP molecule. The shrinking of C—N bond lengths in the $NH_2^+$ group from 1.40 Å to1.33 Å and the contraction bond angle of bond angles of $N_{20}$—$C_{26}$—$N_{18}$ from $119^0$ to $110^0$, the contraction of $NH_3^+$ bond angle $H_{34}$—$N_{17}$—$H_{35}$ from $108^0$ to$103^0$ and the shrinking of C—N bond length from 1.52 Å to 1.49 Å) in the L-argininium cation suggests the twisted Intermolecular charge transfer (TICT) interactions in the LADP molecule [57–59].

### 3.9. Natural Bond Orbital (NBO) analysis

The NBO analysis was performed on the donor-acceptor intermolecular charge transfer interactions via N—H…O and O—H…O hydrogen bonding in the cation-anion complex. The second order perturbation energies $E^{(2)}$ of the acceptor oxygen lone pairs in hydrogen phosphate anion into the N—H and O—H antibonding orbitals are shown in Table TS3(Supplementary Information). The hyperconjugative interactions $LP_2(O_{12})\rightarrow\sigma^*(O_3—H_6)$ and $LP_1(O_{12})\rightarrow\sigma^*(N_{17}—H_{34})$ having stabilization energies 10.63 and 7.14 kcal/mol, results in $O_3$—$H_6$…$O_{12}$ and $N_{17}$—$H_{34}$…$O_{12}$ intermolecular interactions respectively. Likewise, the hydrogen bond occurred between $LP_1(O_9)\rightarrow\sigma^*(N_{18}—H_{37})$ and $LP_1(O_9)\rightarrow\sigma^*(N_{20}—H_{40})$ with stabilization energies 3.68 and 3.29 kcal/mol results in $N_{18}$—$H_{37}$ ….$O_9$ and $N_{20}$—$H_{40}$…$O_9$ intermolecular interactions respectively. These two three-bonded intermolecular interactions are responsible for the charge transfer through LP→σ* between the anion and cations. The other intermolecular interaction identified is $LP_3(O_4)\rightarrow\sigma^*(N_{17}—H_{35})$ which stabilizes with 9.83 kcal/mol and results in $N_{17}$—$H_{35}$…$O_4$ intermolecular

**Table 2**
Nonlinear optical parameters obtained from Z-scan measurement for pure and doped LADP crystals with an error of ± 3% in $n_2$ and ± 0.5% in β.

| | $n_2$ x $10^{-8}$ $cm^2$/W | β x $10^{-4}$ cm/W | Re $\chi^{(3)}$ x $10^{-6}$ esu | Linear refractive index ($n_0$) | Im $\chi^{(3)}$ x $10^{-6}$ esu | $\chi^{(3)}$ x $10^{-6}$ esu | Limiting Threshold (mW) | Clamping value (mW) | Molecular second hyperpolarizability (γ) x $10^{-34}$ esu | Figure of merit |
|---|---|---|---|---|---|---|---|---|---|---|
| LADP | 7.25 | 0.01 | 1.94 | 1.03 | 0.04 | 1.94 | 23.27 | 4.4 | 6.649 | 1362.78 |
| CVLADP | 7.60 | 0.02 | 2.03 | 1.03 | 0.14 | 2.04 | 23.43 | 4 | 6.92 | 714.28 |

interaction. The high electron densities of 0.03085e (σ*($N_{17}$—$H_{34}$)), 0.02919e (σ*($N_{17}$—$H_{35}$)) and 0.03735e (σ*($O_3$—$H_6$)) shows elongation of the corresponding bonds. The low electron density of σ*($N_{20}$—H40) (0.01204e) compared to bifurcated hydrogen bonded σ*($N_{18}$—$H_{37}$) (0.01781e) shows the contraction of $N_{20}$—$H_{40}$ bond. The hyperconjugative interactions and electron density charge transfer in LADP molecule is the origin of blue or red shifting hydrogen bonds [66].

### 3.10. Hirshfeld surface analysis

Hirshfeld surface and fingerprint plots indicate the presence of intermolecular interactions within the crystal structure [49,50]. The normalized contact distance, $d_{norm}$ in terms $d_i$ and $d_e$ of Hirshfeld surface are well correlated with fingerprint plots [28]. Fig. 10(a) shows that the deep red spots indicate N—H···O intermolecular interactions involving the N—H bond in the guanidyl group and $NH_3^+$ group of L-argininium cation with oxygen atoms in the dihydrogen phosphate anions and O—H···O intermolecular interactions within the O—H bonds in the hydrogen phosphate anions. The fingerprint plots show the strong intermolecular contacts such as O···H (31.8%)/H···O (30.7%) and H—H (31.8%). The deep red colour on the O—H sites of the hydrogen phosphate molecule in the $d_{norm}$, the two spikes on the fingerprint plot for strong hydrogen bonding interactions of O···H/H···O, a pale orange spot in the yellow background in the shape index and blue patches in the curvedness plot, as indicated in Fig. 9(b) supports the three-bonded hydrogen bonding in $NH_3^+$ and dihydrogen phosphate molecules inter contacts form two N—H···O intermolecular interactions. Similarly, the N—H···O contacts in N—H group in the the gunidyl part of L-argininium cations with oxygen atoms in the hydrogen phosphate molecule is evident from $d_{norm}$, curvedness and shape index plots on the Hirshfeld surface.

### 3.11. Electron - hole transport properties: evidence to NLO & OLED

Electron-hole transfer rate depends on the structural factors such as the degree of conjugation between the donor - acceptor sites in organic molecules. The vertical and adiabatic electron affinities (VEA & AEA), vertical and adiabatic ionization potential (VIP & AIP) and electron – hole reorganization energies ($\lambda_{electron}$ & $\lambda_{hole}$) are important parameters for the evaluation of the transport rates of holes and electrons. The electron-hole reorganization energies and vertical and adiabatic electron affinities can be defined as follows [75]:

$$\lambda_{electron} = (E_0^- - E_-^-) + (E_-^0 - E_0^0) \quad (1)$$

$$AEA = E_-^- - E_0^0 \quad (2)$$

$$VEA = AEA + (E_0^- - E_-^-) \quad (3)$$

where $E_0^0$ and $E_-^-$ are the optimized energy of the neutral and anionic states, and $E_0^-$ and $E_-^0$ are the energy of the neutral molecule at the anionic state and the energy of the anionic molecule at the neutral state.

$$\lambda_{hole} = (E_0^+ - E_+^+) + (E_+^0 - E_0^0) \quad (4)$$

$$AIP = E_+^+ - E_0^0 \quad (5)$$

$$VIP = AIP + (E_0^+ - E_+^+) \quad (6)$$

where $E_0^0$ and $E_+^+$ are the optimized energy of the neutral and cationic states, and $E_0^+$ and $E_+^0$ are the energy of the neutral molecule at the cationic state and the energy of the anionic molecule at the neutral state.

The basic requirements for high quantum efficiency OLED materials possess high electron mobility and low reorganization energy [63]. The calculated values as shown in Table 5 reveal that the value of $\lambda_{electron}$ is smaller than that of $\lambda_{hole}$. This result is necessary for OLED material, suggests that the electron transfer rate is better than that of the hole transfer rate [63]. The LADP complex possesses good electron transport

**Table 3**
Comparison of static and field dependent first & second hyperpolarizability, polarizability, and dipole moment for the pristine and LADP molecules are calculated with DFT/B3LYP/6-31 + + G (d,p).

| | | L-Arginine | Phosphoric acid | LADP |
|---|---|---|---|---|
| μtotal (Debye) | | 15.16 | 4.30 | 17.79 |
| $\alpha(0,0)\times10^{-24}$ esu | $\alpha_{total}$ | 16.07 | 4.50 | 28.05 |
| | $\Delta\alpha$ | 6.97 | 0.77 | 8.05 |
| $\alpha(-\omega,\omega)\times10^{-24}$ esu | $\alpha_{total}$ | 16.65 | 4.62 | 29.42 |
| | $\Delta\alpha$ | 7.51 | 0.78 | 9.06 |
| $\beta(0;0,0)\times10^{-30}$ esu | | 1.27 | 0.18 | 2.00 |
| $\beta(-\omega;\omega,0)\times10^{-30}$ esu | | 2.97 | 0.29 | 112.27 |
| $\beta(-2\omega;\omega,\omega)\times10^{-30}$ esu | | 4.45 | 0.34 | 17.26 |
| $\gamma(0;0,0,0)\times10^{-36}$ esu | | 11.59 | 0.78 | 15.85 |
| $\gamma(-\omega;\omega,0,0)\times10^{-36}$ esu | | 14.95 | 0.89 | 1508.64 |
| $\gamma(-2\omega;\omega,\omega,0)\times10^{-36}$ esu | | −843.64 | 1.19 | 19.82 |

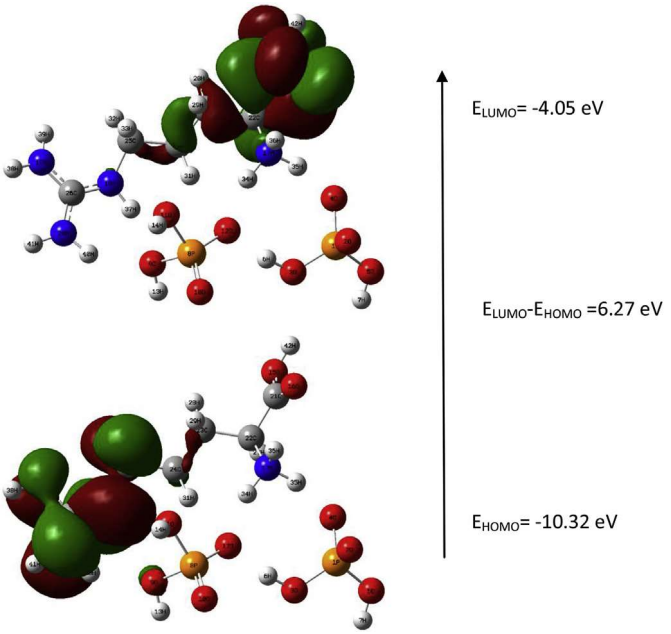


**Fig. 8.** Frontier molecular orbitals (HOMO and LUMO) of LADP.

properties and it is useful in light emitting materials with high quantum efficiency. The negative value of VEA denotes the unbound nature of anionic state [72].

**Table 4**
Hydrogen bond geometry in LADP.

| D-H … A (Å) | D-H(Å) | H ….A (Å) | D ….A(Å) | D-H …..A (°) |
|---|---|---|---|---|
| $N_{17}$—$H_{34}$ ….$O_{12}$ | 1.05 | 1.73 | 2.75 | 160.74 |
| $N_{17}$—$H_{35}$ …..$O_4$ | 1.04 | 1.73 | 2.75 | 162.91 |
| $O_3$—$H_6$···$O_{12}$ | 1.01 | 1.62 | 2.62 | 170.34 |
| $N_{20}$—$H_{40}$ …..$O_9$ | 1.02 | 2.03 | 2.93 | 146.55 |
| $N_{18}$—$H_{37}$ …..$O_9$ | 1.02 | 1.99 | 2.92 | 149.96 |

### 3.12. Vibrational analysis

The FT-IR and FT-Raman spectra were analysed on the basis of characteristic vibrations of L-arginine cations and dihydrogen phosphate anions. The theoretical assignments of the bands given by Normal Coordinate Analysis (NCA) was followed by the recommendations of Fogarasi and Pulay [25,26]. The experimental infrared and Raman bands and the calculated harmonic wavenumbers with their corresponding potential energy distributions (PED) are given in Table 6. The theoretically simulated infrared and Raman spectra with corresponding experimental FT-IR and FT-Raman spectra of LADP crystal resulted with RMS deviation of 14.3 $cm^{-1}$ are shown in Fig. 11&Fig. 12.

#### 3.12.1. L-Argininium cation vibrations

The guanidyl part of the L-argininium cation consisting of $NH_2$ and $NH_2^+$ functional groups are strongly involved in hydrogen bonding interaction with the oxygen atom of the bis dihydrogen phosphate anion forming N—H ….O hydrogen bond, which can shift the position of N—H stretching and bending vibrations. The NH stretching vibrations were expected around 3350 -2700 $cm^{-1}$ [29]. The optimized bond length for $N_{20}$—$H_{40}$ bond in the $NH_2^+$ group were shortened by 0.005 Å, which manifests the $N_{20}$—$H_{40}$···$O_9$ intermolecular interaction. The vibrational spectra of LADP crystal show strong bands at 3421 $cm^{-1}$ FT-IR which can be assigned for $H_{41}$—$N_{20}$—$H_{40}$ ($NH_2^+$) asymmetric and symmetric stretching vibrations. In the DFT calculation, $NH_2^+$ stretching wavenumbers of the L-argininium and the LADP molecules were 3643 and 3673 $cm^{-1}$, respectively, which implies 30 $cm^{-1}$ blue shift of the N—H stretching wavenumbers in LADP. It should be emphasized that this result is completely different from the similar L-argininium compound which shows $NH_2^+$ asymmetric and symmetric stretching wavenumbers at 3333 & 3156 [74] and 3175 & 3000 $cm^{-1}$ [52] respectively. Moreover, the decrease in the intensity of the N—H stretching band as revealed from the calculations, confirms the presence of $NH_2^+$ …..$O_9$ intermolecular blue-shifting hydrogen bond in LADP [76,77]. Whereas, the band present at 3379 $cm^{-1}$ is assigned to the asymmetric stretching vibration of $NH_2$ group ($H_{38}$—$N_{19}$—$H_{39}$). The experimental values of symmetric and asymmetric stretching vibrations of $NH_2^+$ are blue shifted by 42 $cm^{-1}$ compared to

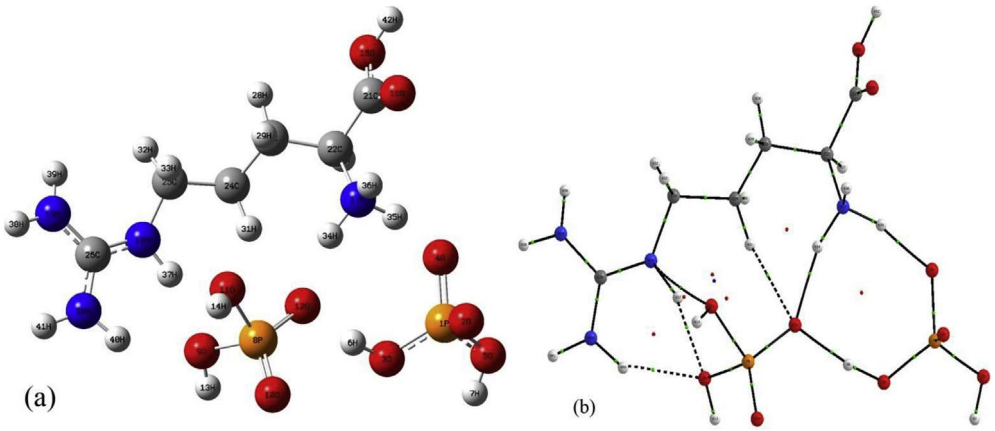


**Fig. 9.** (a) Optimized geometry (b) Molecular graph at BCP of LADP by B3LYP/6-31 + + G (d,p) basis set.

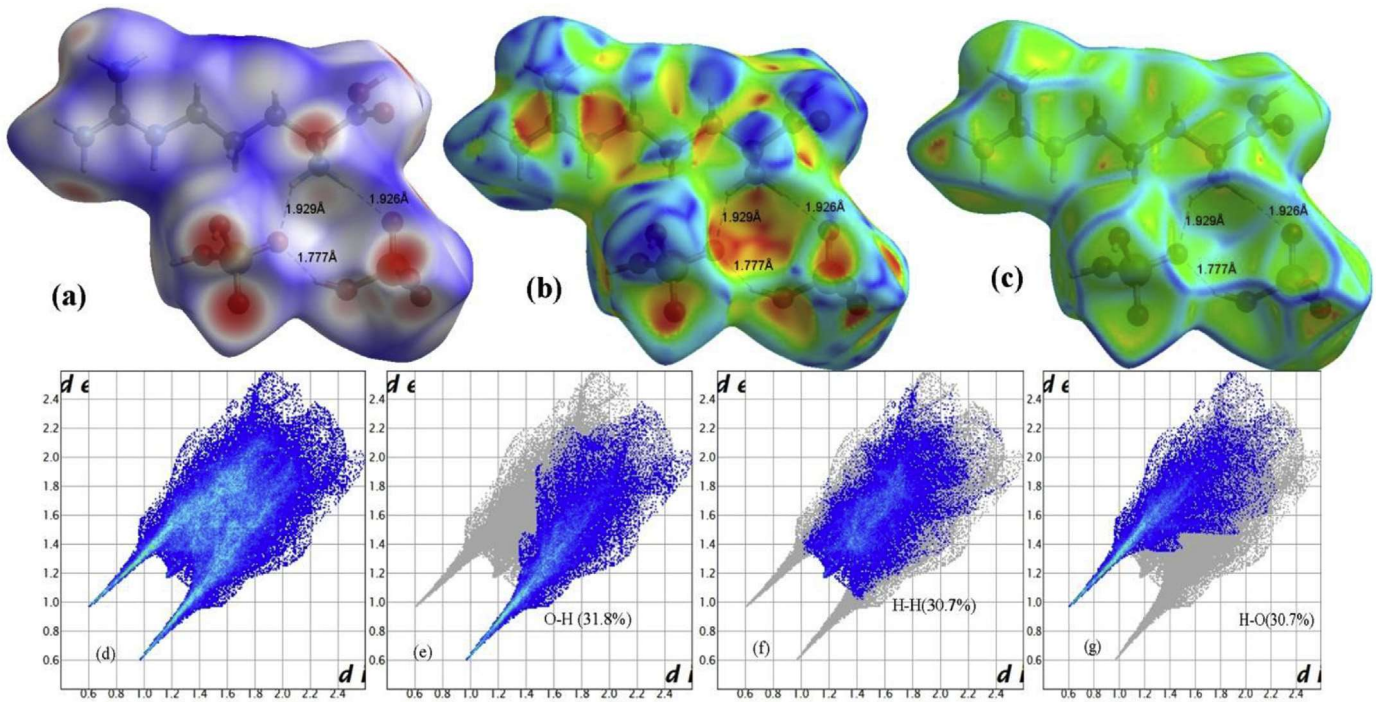


**Fig. 10.** (a)$d_{norm}$ surface (b) Curvedness (c) shape index surfaces of LADP (d), (e), (f) and (g) bearing two-dimensional fingerprint plots for LADP molecule. Various close contacts and their relative contributions are indicated.

**Table 5**
Ionization potentials (VIP & AIP), electron affinities (VEA & AEA), reorganization energies calculated at B3LYP/6-31 + + G (d,p) level.

| VEA (a.u) | AEA (a.u) | AIP (a.u) | VIP (a.u) | $\lambda_{electron}$ (a.u) | $\lambda_{hole}$ (a.u) |
|---|---|---|---|---|---|
| −0.019 | 0.038 | 0.285 | 0.322 | 0.025 | 0.120 |

that of $NH_2$. The $N_{18}$—$H_{37}$ stretching band is identified at 3328 $cm^{-1}$ with PED contribution of 82%. In DFT calculation, NH stretching wavenumbers of the L-argininium molecule and the LADP complex were 3562 and 3437 $cm^{-1}$, respectively, which implies 125 $cm^{-1}$ redshift of N—H stretching wavenumbers due to the $N_{18}$—$H_{37}$···$O_9$ intermolecular interaction. The corresponding asymmetric band of CVLADP crystal was at 3425 $cm^{-1}$ for $H_{41}$—$N_{20}$—$H_{40}$ stretching in the FT-IR spectra while the symmetric stretching band was absent in the FT-Raman spectra, whereas for $H_{38}$—$N_{19}$—$H_{39}$ symmetric stretching vibrations the bands were observed at 3377 $cm^{-1}$ in FT-IR and 3366 $cm^{-1}$ in FT-Raman spectrum, which also confirms the blue shifting. The symmetric deformation bands of $NH_2$ group generally appear in the range 1638–1575 $cm^{-1}$ [50]. The bands appeared at 1629 $cm^{-1}$ in FT-IR and 1574 $cm^{-1}$ in FT-Raman are assigned to the symmetric deformation modes of LADP with 50% and 30% of PED contributions, respectively. The band observed in the FT-Raman spectra at 1688 $cm^{-1}$ is assigned for asymmetric deformation mode of $NH_2$ group. DFT predicts the asymmetric deformation mode of the L-argininium molecule and the LADP complex at 1652 and 1715 $cm^{-1}$, respectively, which implies 63 $cm^{-1}$ blue shift of the $NH_2$ asymmetric deformation mode in the LADP complex. Whereas, the symmetric deformation mode of the L-argininium molecule is at 1629 $cm^{-1}$ and the LADP complex was at 1700, 1647 and 1610 $cm^{-1}$, respectively, which implies blue shift of the $NH_2$ symmetric deformation mode in the LADP complex [71]. In the case of CVLADP, the symmetric deformation mode appeared at 1628 $cm^{-1}$ in FT-IR which is found to be overlapping with the C—N stretching vibrations of guanidyl group. In the case of CVLADP, the symmetric deformation mode appeared at 1628 FT-IR $cm^{-1}$ which is found to be overlapping with the C—N stretching vibrations of guanidyl group. The bands due to the $NH_2$ rocking modes were identified at 1068 FT-Raman, 1441 FT-Raman and 529-FT-IR, 526 $cm^{-1}$ -FT-Raman for LADP crystal, and 1052 FT-Raman, 1450 FT-Raman and 519 FT-IR, 528 $cm^{-1}$ -FT-Raman for CVLADP crystal.

The bands corresponding to the asymmetric and symmetric stretching vibrations of $NH_3^+$ group are expected in the ranges 3300-3100 $cm^{-1}$ and 3100-2600 $cm^{-1}$, respectively [44]. NCA treats the $NH_3^+$ stretching bands in LADP molecule as an individual N—H stretching vibration because of the N—H···O interactions with the oxygen atom in the dihydrogen phosphate molecule. The strong FT-IR band at 3194 $cm^{-1}$ is assigned for $N_{17}$—$H_{36}$ stretching vibration and Raman bands at 2925 for $N_{17}$—$H_{34}$ and at 2919 $cm^{-1}$ for $N_{17}$—$H_{35}$ stretching vibrations. In DFT calculation, $NH_3^+$ stretching wavenumbers of L-argininium molecule is at 3501 and 3269 $cm^{-1}$, and that for LADP complex were at 3425, 3034 and 2991 $cm^{-1}$, respectively, which implies red shift of the N—H stretching wavenumbers in LADP. The $N_{17}$—$H_{34}$ ….$O_{12}$ and $N_{17}$—$H_{35}$···$O_4$ intermolecular interactions confirms the red shifting of $NH_3^+$ stretching vibrations. The red shifting of $NH_3^+$ stretching vibrations of LADP emphasises that the result is completely different from the other L-arganinium compounds which appeared at 3075 [52] and 3205 $cm^{-1}$ [78]. The $NH_3^+$ asymmetric and symmetric deformation bands are generally expected in the ranges 1660–1610 and 1550-1485 $cm^{-1}$ respectively [30]. The weak FT-IR band in LADP at 1648 $cm^{-1}$ is assigned to the asymmetric deformation of $NH_3^+$ group which is found to be coupled with C—N stretching. The medium strong band identified at 1529 $cm^{-1}$ for symmetric deformation vibration is theoretically predicted with 56% of PED contribution. The $NH_3^+$ rocking mode is identified at 1160 $cm^{-1}$ in the FT-IR spectrum of LADP crystal which is calculated with PED of 13%. The asymmetric deformation mode of the L-argininium molecule and the LADP complex were predicted by DFT at 1809 and 1707 $cm^{-1}$, respectively, which implies 102 $cm^{-1}$ redshift of the $NH_3^+$ asymmetric deformation mode in the LADP complex. Whereas, the symmetric deformation mode of the L-argininium molecule is at 1633 $cm^{-1}$ and the LADP complex were at 1651, 1607 $cm^{-1}$, respectively, which implies redshift of the $NH_3^+$ symmetric deformation mode in the LADP complex [71].

**Table 6**
Experimental FT-IR, Raman and theoretical wavenumbers in ($cm^{-1}$) assignments and PED contributions of LADP and CVLADP crystal by NCA based on SQM force field calculations.

| FT-IR[a] | FT-Raman[a] | FT-IR[b] | FT-Raman[b] | unscaled | scaled[c] | Vibrational assignments PED (%) |
|---|---|---|---|---|---|---|
| | | | | 3774 | 3692 | $\upsilon(O_{15}—H_{42})$ (100) |
| | | | | 3767 | 3502 | $\upsilon(O_{11}—H_{14})$ (100) |
| | | | | 3751 | 3495 | $\upsilon(O_{9}—H_{13})$ (100) |
| | | | | 3713 | 3480 | $\upsilon(O_{5}—H_{7})$ (100) |
| 3425s | | 3421s | | 3673 | 3417 | $\upsilon_{as}$ ($N_{20}—H_{40}—H_{41}$) (78), $\upsilon_{s}$ ($N_{20}—H_{40}—H_{41}$)(21) |
| 3377 ms | | 3379 ms | | 3595 | 3354 | $\upsilon_{s}$ ($N_{19}—H_{38}—H_{39}$) (83), $\upsilon_{as}$ ($N_{19}—H_{38}—H_{39}$)(85), |
| | | | | 3472 | 3339 | $\upsilon_{s}$ ($N_{19}—H_{38}—H_{39}$)(85), $\upsilon(N_{18}—H_{37})$(14) |
| | | | 3328w | 3437 | 3326 | $\upsilon_{s}$ ($N_{18}—H_{37}$)(82) |
| 3194s | | 3194s | | 3425 | 3199 | $\upsilon(N_{17}—H_{36})$(100) |
| | | | | 3115 | 3027 | υ(CH)(97) |
| | | | 3010w | 3110 | 3002 | $\upsilon_{as}$ ($CH_2$) (82) |
| | | | | 3090 | 2974 | $\upsilon(NH_3)$ (90) |
| | | | | 3075 | 2971 | $\upsilon_{as}$ ($CH_2$)(84), $\upsilon_{s}$ ($CH_2$)(13) |
| | 2955s | | 2951s | 3055 | 2955 | $\upsilon_{as}$ ($CH_2$) (77), $\upsilon_{s}$ ($CH_2$) (19) |
| | | 2935 | | 3037 | 2940 | $\upsilon_{s}$ ($CH_2$)(59), $\upsilon_{as}$ ($CH_2$)(33) |
| | 2925s | | | 3034 | 2923 | υ ($N_{17}—H_{34}$) (74), υ ($N_{18}—H_{37}$) (12), υ (CH) (10) |
| | | | 2919s | 3032 | 2916 | υ ($N_{17}—H_{35}$)(81), $\upsilon_{as}$ ($CH_2$) (11) |
| | | | | 2991 | 2911 | $\upsilon_{s}$ ($CH_2$)(96) |
| 2643w | 2650w | 2643w | 2631w | 2873 | 2631 | υ ($O_3—H_6$) (88), υ ($O_{12}—H_6$) (6) |
| 1723 ms | 1715w | 1718w | 1729w | 1827 | 1729 | $\upsilon_{as}$ ($CO_2$)(60) |
| | | | 1688w | 1715 | 1658 | $\delta_{as}$ ($NH_2$) (47), υ (CN) (14) |
| 1659w | 1659w | 1648w | | 1707 | 1656 | $\delta_{as}$ ($NH_3$)(28), υ (CN)(22), ρ($N_{18}—H_{37}$)(13) |
| 1628s | | 1629s | | 1700 | 1643 | $\delta_{s}$ ($NH_2$) (50), υ (CN) (34) |
| | | | | 1651 | 1599 | $\delta_{as}$ ($NH_3$)(57), τ($O_3—H_6$) (17) |
| | | | | 1647 | 1596 | $\delta_{s}$ ($NH_2$) (55), ρ($N_{18}—H_{37}$) (19), υ (CN) (18) |
| | | | 1574w | 1610 | 1562 | υ (CN) (38), $\delta_{s}$ ($NH_2$) (30), ρ(GU) (12), ρ($NH_2$) (11) |
| 1531 ms | | 1529 ms | | 1607 | 1544 | $\delta_{s}$ ($NH_3$) (56), τ($O_3—H_6$) (28) |
| | | | 1519 | 1524 | 1485 | γ($CH_2$) (85) |
| | | | | 1513 | 1474 | γ($CH_2$) (89) |
| 1467 ms | | 1465 ms | | 1496 | 1463 | γ($CH_2$) (93) |
| | 1450 ms | | 1441 ms | 1477 | 1434 | υ (CN) (29), ρ($N_{18}—H_{37}$) (26), ω($CH_2$) (14) |
| 1397w | | 1404w | 1411w | 1455 | 1413 | ω($CH_2$) (62), β(OH) (11) |
| | | | | 1434 | 1385 | ρ($CH_2$) (30), δ($C_{22}—H_{27}$) (18), υ (CC) (11) |
| | 1374w | | 1362 ms | 1399 | 1364 | ω($CH_2$) (63) |
| 1335 ms | | 1333 ms | | 1375 | 1340 | Γ($CH_2$) (32), ω($CH_2$) (23) |
| | 1331 ms | | 1328 ms | 1360 | 1325 | Γ($CH_2$) (41), ρ($CH_2$) (14), β(OH) (10), ω($CH_2$) (10) |
| | | | | 1334 | 1301 | ω($CH_2$)(47), Γ($CH_2$) (22) |
| | | | | 1324 | 1294 | Γ($CH_2$)(52), ω($CH_2$)(12) |
| 1281 ms | 1282w | 1283mss | 1285w | 1318 | 1279 | β(OH) (76), τ($O_3—H_6$) (15) |
| | | | | 1287 | 1246 | δ($C_{22}—H_{27}$)(24), ω($CH_2$)(21), Γ($CH_2$) (17) |
| 1234w | | 1233w | | 1278 | 1229 | υ (PO) (36), β(OH) (16), Γ($CH_2$) (14) |
| | | | | 1259 | 1226 | υ (PO) (24), Γ($CH_2$) (20), β(OH) (11) |
| | | | 1160s | 1200 | 1165 | ρ($CH_2$) (26), Γ($CH_2$) (17), ρ($NH_3$) (13) |
| | | | | 1192 | 1146 | υ (CN) (45), ρ($NH_2$) (33) |
| | | | | 1178 | 1138 | ρ($NH_3$) (22), $\upsilon_{s}$ ($CO_2$) (12) |
| 1108s | | 1116s | | 1152 | 1103 | β(OH) (65) |
| | | | | 1141 | 1096 | $\upsilon_{s}$ ($CO_2$) (18), δ($C_{22}—H_{27}$)(14), β(OH) (11), $\upsilon_{as}$ ($CO_2$)(10) |
| | | | | 1119 | 1086 | υ (PO)(65), β(OH) (23) |
| | | | | 1110 | 1078 | υ (CN)(22), Γ($CH_2$)(15), ρ($NH_2$) (13) |
| | 1052 ms | | 1068 ms | 1095 | 1066 | ρ($NH_2$) (52), υ (CN) (29) |
| | | | | 1083 | 1055 | β(OH) (78), υ (PO)(12) |
| | | | | 1071 | 1054 | ρ($NH_2$) (23), ρ($CH_2$) (18), υ (CN) (15), ρ($NH_3$) (11) |
| | | 1037 ms | 1036w | 1070 | 1036 | υ (CC) (31), Γ($CH_2$) (18) |
| 1026s | | | | 1063 | 1030 | υ (CC) (66) |
| | | | 1003w | 1036 | 1000 | υ (CC) (39), υ (CN) (18) |
| 984 ms | 982s | 973w | | 1023 | 974 | β(OH) (54), υ (PO)(40) |
| | | | | 992 | 963 | υ (PO) (58), β(OH) (23) |
| 943 ms | | 945 ms | | 986 | 952 | υ (CN) (39), υ (CC) (20) |
| | | | 924w | 984 | 923 | υ (PO) (76) |
| | 911 ms | | | 952 | 919 | υ (CC) (19), υ (CN) (17), ρ($CH_2$) (14) |
| 876 ms | 884w | 875 ms | 879s | 909 | 869 | τ($O_3—H_6$) (49), τ($P_1—O_3$) (23), β(OH) (18) |
| | | | 850w | 893 | 855 | ρ($CH_2$)(39), υ (CC) (18), Γ($CH_2$)(10) |
| | 811w | | | 885 | 832 | υ (PO) (63) |
| | | | | 857 | 828 | υ (PO)(22), υ (CC) (14), ρ($CH_2$)(12) |
| | | | | 824 | 781 | υ (PO) (44), ω($NH_2$) (15), τ($C_{26}—N_{18}$)(11) |
| 765w | | 764w | | 823 | 769 | υ (PO) (91) |
| 741w | 744w | | | 779 | 748 | υ (PO)(32), ω($NH_2$) (22), τ($C_{26}—N_{18}$) (18) |
| | | | | 758 | 736 | ω($CO_2$) (31), τ($C_{21}—O_{15}$) (17), ρ($CH_2$) (13) |
| | | | | 747 | 720 | ρ($CH_2$)(44), τ($C_{25}—C_{24}$) (14), τ($C_{24}—C_{23}$) (11) |
| | | | | 722 | 698 | ω(GU) (73) |
| | | | | 717 | 691 | υ (PO)(27), β(OH) (17), ω($NH_2$) (12) |
| | | | | 686 | 662 | υ (PO) (59) |
| | 654w | | 669w | 664 | 645 | τ($C_{21}—O_{15}$) (43), δs ($CO_2$) (21) |

(*continued on next page*)

**Table 6** (*continued*)

| FT-IR[a] | FT-Raman[a] | FT-IR[b] | FT-Raman[b] | unscaled | scaled[c] | Vibrational assignments PED (%) |
|---|---|---|---|---|---|---|
| 621w | 592w | 616w | | 641 | 624 | τ($C_{21}$—$O_{15}$) (22), δs ($CO_2$) (22) |
| | | | | 579 | 559 | δ(GU) (36), δ($N_{18}$—$H_{37}$) (16) |
| 519 ms | 528 ms | 529 ms | 526 ms | 536 | 523 | ρ(GU) (52), Γ($CH_2$)(19), υ(O—H) (10) |
| | | | | 526 | 516 | υ(O—H) (16), β(OH) (11) |
| 498w | | | | 503 | 489 | β(OH) (26), δs (PO) (18) |
| | | | | 489 | 477 | δas (PO) (24), β(OH) (18), τ($P_8$—$O_9$) (10) |
| | | | | 483 | 469 | τ($N_{19}$—$C_{26}$) (22), β(OH) (18), ω($NH_2$) (15) |
| | | | | 478 | 463 | β(OH) (27), τ($N_{17}$—$C_{22}$) (14), δas (PO) (14) |
| | | | | 472 | 459 | δas (PO)(31), β(OH) (20) |
| | | | | 454 | 442 | δs (PO) (29), τ($N_{17}$—$C_{22}$) (17) |
| | | | | 440 | 432 | τ($N_{17}$—$C_{22}$) (27), ρ(PO) (13), τ($P_8$—$O_{11}$) (12) |
| | 411w | | | 426 | 417 | δs (PO)(56), τ($P_1$—$O_{14}$) (14) |
| 408w | | | | 412 | 399 | Γ($CH_2$)(22), β(OH) (20) |
| | | | 395w | 407 | 395 | τ($P_8$—$O_{11}$)(27), Γ($CH_2$) (13) |
| | | | | 394 | 384 | δas (PO) (16), υ(O—H)(12), β(OH) (11) |
| | | | | 390 | 369 | ω($NH_2$) (50), τ($N_{20}$—$C_{26}$) (30) |
| | | | 361 ms | 378 | 363 | τ($N_{17}$—$C_{22}$) (28), τ($O_3$—$H_6$) (18), υ(O—H)(11) |
| | | | | 347 | 337 | ρ(PO) (38), τ($P_1$—$O_5$) (28) |
| | | | | 344 | 330 | τ($N_{20}$—$C_{26}$) (16), Γ($CH_2$) (15), ω($NH_2$) (15), υ(O—H)(10) |
| | | | | 334 | 322 | ρ(PO) (18), τ($N_{20}$—$C_{26}$) (14), ω($NH_2$) (14), δas (PO) (13) |
| | | | | 325 | 314 | ρ($CO_2$) (16), υ(O—H)(14) |
| | | | | 319 | 305 | ω($NH_2$) (37), τ($N_{20}$—$C_{26}$) (31) |
| | | | | 315 | 304 | ω($NH_2$) (23), ρ(PO)(23), τ($N_{20}$—$C_{26}$) (20) |
| | | | 254w | 281 | 267 | τ($P_8$—$O_9$) (25), δas (PO) (20), ρ(PO) (10) |
| | 232w | | | 235 | 230 | τ($P_1$—$O_5$) (24), υ(O—H)(19), ρ(PO)(11) |
| | | | | 215 | 212 | υ(O—H)(22), Γ($CH_2$) (20) |
| | | | | 193 | 189 | υ(O—H)(19), δ($N_{18}$—$H_{37}$) (10), τ($P_1$—$O_5$) (10) |
| | | | | 173 | 169 | υ(O—H)(17), β(OH) (16) |
| | | | | 161 | 161 | υ(O—H)(38), τ($C_{23}$—$C_{22}$) (14) |
| | | | | 160 | 150 | υ(O—H)(27), ω($NH_2$) (15), τ($C_{25}$—$C_{24}$)(15), τ($C_{26}$—$N_{18}$) (14) |
| | | | | 148 | 146 | τ($C_{25}$—$C_{24}$) (34), υ(O—H)(14) |
| | | | | 143 | 139 | β(OH) (33), υ(O—H)(17) |
| | | | | 127 | 128 | υ(O—H)(20), τ($C_{24}$—$C_{23}$) (15), β(OH) (12) |
| | | | | 109 | 112 | υ(O—H)(25), β(OH) (12), τ($C_{25}$—$N_{18}$) (10) |
| | | | | 102 | 98 | ω($NH_2$) (32), β(OH) (25), τ($C_{26}$—$N_{18}$)(15) |
| | | | | 101 | 94 | β(OH) (29), τ($C_{23}$—$C_{22}$) (24), τ($C_{25}$—$C_{24}$) (21) |
| | | | | 90 | 82 | β(OH) (32), τ($C_{23}$—$C_{22}$) (16), τ($C_{25}$—$C_{24}$) (14) |
| | | | | 81 | 76 | β(OH) (51), τ($P_1$—$O_{14}$) (11) |
| | | | | 66 | 61 | β(OH) (26), τ($C_{23}$—$C_{22}$) (15), τ($C_{25}$—$C_{24}$) (11), τ($C_{25}$—$N_{18}$) (10) |
| | | | | 54 | 48 | β(OH) (53), τ($P_8$—$O_{12}$) (12), τ($P_1$—$O_{14}$) (11) |
| | | | | 48 | 45 | β(OH) (50), τ($C_{25}$—$N_{18}$) (14) |
| | | | | 46 | 40 | τ($O_3$—$H_6$) (34), β(OH) (20), τ($P_1$—$O_{14}$) (15), τ($C_{25}$—$N_{18}$) (14) |
| | | | | 45 | 38 | τ($C_{25}$—$N_{18}$) (45), τ($N_{17}$—$C_{22}$) (12) |
| | | | | 43 | 34 | β(OH) (68) |
| | | | | 37 | 29 | τ($C_{25}$—$C_{24}$) (44), β(OH) (25), τ($C_{25}$—$N_{18}$) (12) |
| | | | | 31 | 24 | τ($P_1$—$O_{14}$) (43), β(OH) (18), τ($C_{25}$—$C_{24}$) (14) |
| | | | | 20 | 16 | β(OH) (38), τ($C_{25}$—$C_{24}$) (21), τ($N_{17}$—$C_{22}$) (14), τ($P_8$—$O_{12}$)(10) |

υ: stretching, γ: scissoring, ω: wagging, τ: torsion, Γ: twisting, β: in-plane bending, δ: deformation, ρ:rocking, s: symmetric, as: antisymmetric, GU: guanidyl group, vs: very strong, s: strong, ms: medium strong, w: weak.

[a] CVLADP crystal.

[b] LADP crystal.

[c] the wavenumbers obtained at B3LYP/6-31 + +G (d,p) level were scaled using NCA based on SQM Force field Calculations.

The vibrational spectral studies of characteristic bands in the carboxylate group give the strength of the hydrogen bonding in the crystal structure [51]. The stretching vibrations of carbonyl C—O group generally appear in the region 1780-1700 $cm^{-1}$ [30]. The band present in the FT-IR spectrum of LADP at 1718 $cm^{-1}$ is assigned to C—O group stretching vibrations, which is also seen as a weak band in the FT-Raman spectrum at 1729 $cm^{-1}$. Similar to the case of LADP, sharp bands present at 1723 and 1715 $cm^{-1}$ in FT-IR and FT-Raman spectra, respectively are assigned to the stretching vibrations of the carbonyl group of CVLADP. The in-plane bending of C—O—H is observed at 1328 $cm^{-1}$ for LADP whereas at 1331 $cm^{-1}$ as an intense FT-Raman band for CVLADP. The carboxylate symmetric deformation bands were identified for LADP at 616 FT-IR & 669 FT-Raman $cm^{-1}$ and 621FT-IR (592-FT-Raman) & 654 $cm^{-1}$ for CVLADP. Figs. 11 and 12 show that CVLADP reflects more intense bands than LADP spectra of carboxylate group vibrations which confirms the increase in the conjugation and formation of hydrogen bonding due to the doping of crystal violet in the LADP [52–54].

The $CH_2$ asymmetric and symmetric stretching vibrations occur in the regions 3100–3000 and 3000-2900 $cm^{-1}$ respectively [55–57]. The sharp and moderate intense Raman active bands present at 2951 and 3010 $cm^{-1}$ are assigned for $CH_2$ asymmetric stretching vibrations with 77 and 82% of PED contribution in LADP. The symmetric stretching band is present at 2935 $cm^{-1}$in FT-IR and 2919 $cm^{-1}$ in FT-Raman spectrum for LADP crystal. The variation in the wavenumbers of $CH_2$ vibrations from the expected range is due to the electronic back donation of the nitrogen atom in the adjacent side of the methylene group [52]. The characteristic band of scissoring mode of $CH_2$ group is identified at 1465 in FT-IR [53] and 1519 $cm^{-1}$ in FT-Raman spectra of LADP with 93 and 85% of PED contribution. The strong band in the FT-Raman spectrum at 1160 $cm^{-1}$ and moderate band at 850 $cm^{-1}$ is assigned for rocking vibration of $CH_2$ group. The $CH_2$ wagging modes identified at 1141, 1404, 1333 in FT-IR spectrum and 1411, 1362, 1328 $cm^{-1}$are coupled with C—H rocking mode in FT-Raman spectrum

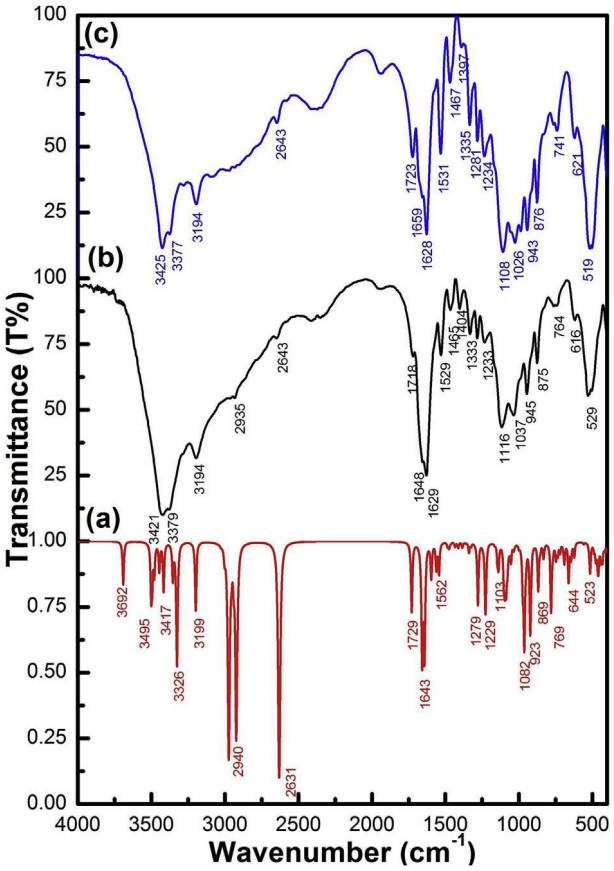


**Fig. 11.** (a) Simulated IR spectra of LADP molecule (b) Experimental FTIR spectra of pure LADP (c) Experimental FTIR spectra of doped LADP crystals.

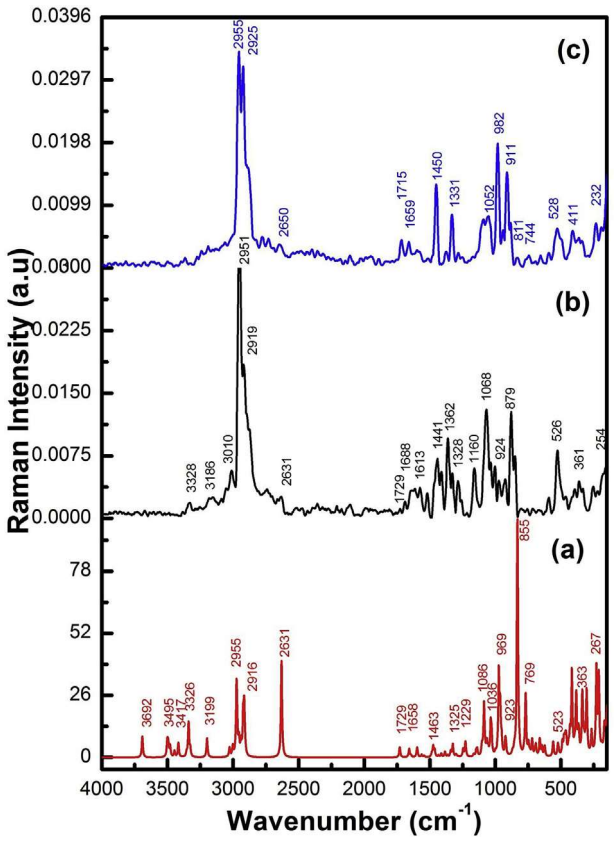


**Fig. 12.** (a) Simulated Raman spectra of LADP molecule (b) Experimental FT-Raman spectra of pure LADP (c) Experimental FT-Raman spectra of doped LADP crystals.

of LADP. $CH_2$ twisting band is observed at 1333 and 1233 $cm^{-1}$ in FT-IR and 1328 and 1160 $cm^{-1}$ in FT-Raman spectrum. The rocking, wagging and twisting vibrational bands were identified and assigned for CVLADP crystal.

The double bonded C═N stretching vibrations in the guanidyl group was expected as an intense band near 1689-1657 $cm^{-1}$ [64]. In LADP, the prominent bands at 1688, 1629 and 1574 $cm^{-1}$ in FT-IR spectrum is assigned for C═N stretching vibrations of guanidyl group. The C—N and C—C skeletal mode bands are usually observed in the region 1150-850 $cm^{-1}$ [65,66]. The bands at 1441, 1068, and 1003 $cm^{-1}$ in FT-Raman spectrum and 945 $cm^{-1}$ in FT-IR spectrum are assigned for C—N stretching vibrations. The C—C stretching vibrations assigned for LADP at 1036, 1003 and 850 $cm^{-1}$ in FT-Raman spectrum and 945 $cm^{-1}$ in FT-IR spectrum are coupled with C—N stretching vibrations. The C—C and C—N stretching vibrations assigned for CVLADP shows significant deviation from the LADP, which indicates that doping induces distortion in the skeletal modes of vibrations.

### 3.12.2. Vibrations of dihydrogen phosphate anions

The O—H stretching vibrational mode of the dihydrogen phosphate anion is assigned to the band 2643 $cm^{-1}$ in FT-IR and the corresponding FT-Raman band at 2631 $cm^{-1}$ with PED contribution 88%. The redshifting in the wavenumbers of O—H stretching vibrations confirms the existence of O—H···O intermolecular hydrogen bond [60–62]. The in plane bending of P—O—H is coupled with P—O stretching vibrations. The bands observed at 1404, 1283, 1233, 1116, 973 and 875 $cm^{-1}$ in FT-IR spectrum and 1411, 1285, 973 and 879 $cm^{-1}$ in FT-Raman spectrum are assigned for in-plane bending vibration of P—O—H. The intermolecular interactions of cation and anion manifest shifting of P—O stretching vibrations into different wavenumbers in vibrational spectra. The P—O stretching wavenumbers are observed at 1283, 1233, 973, and 764 $cm^{-1}$ in FT-IR spectrum and 1285 and 924 $cm^{-1}$ in FT-Raman spectrum. Similarly, the in-plane and P—O stretching vibrations assigned in CVLADP crystal, shows new bands at 498-FT-IR, 408-FT-IR, 411 FT-Raman, 741-FT-IR with 744 in FT-Raman and 831 FT-Raman $cm^{-1}$. The bands observed at 254 FT-Raman for LADP and 498 FT-IR and 411 FT-Raman for CVLADP crystal are assigned for asymmetric and symmetric $PO_3$ deformation modes.

### 3.13. AIM analysis

The theory of atoms in a molecule (AIM) measures the strength of the intermolecular hydrogen bond and is analyzed using the values of electron density ($\rho_{(r)}$), their Laplacians ($\nabla^2\rho_{(r)}$) and total electronic energy density (H) at the Bond Critical Points (BCPs) [67]. In LADP molecule, the cation-anion interaction through two three-bonded hydrogen bonds; the oxygen atom $O_9$ bonded with two N—H site of guanidyl group, forms $P_8$—$O_9$···$H_{40}$—$N_{20}$ and $P_8$—$O_9$···$H_{37}$—$N_{18}$ intermolecular hydrogen bonds. $NH_3^+$ group and hydrogen phosphate forms two intermolecular hydrogen bonds $P_8$—$O_{12}$···$H_{34}$—$N_{17}$ and $P_8$—$O_{12}$···$H_6$—$O_3$ as shown in Fig. 9(b). The electron density, $\rho_{(r)}$ values are greater than 0.04 a. u for $O_{12}$···$H_6$, $O_{12}$···$H_{34}$ and $O_4$···$H_{35}$ indicates the covalent nature of these intermolecular hydrogen bonds [68]. The Laplacians ($\nabla^2\rho_{(r)}$) and total energy density (H) are relevant quantities determining the strength of nonbonded intermolecular interactions. The negative values of both Laplacians, $\nabla^2\rho_{(r)}$ and H at their critical points as shown in Table 7 confirms the covalent nature of O ….H intermolecular contacts [69].

The increasing electron density at $BCP_s$ shows a redshift in the wavenumber bands in the corresponding bond vibrations [57]. Pure and doped LADP vibrational spectrums shows O—H stretching bands theoretically calculated at 2361 for $O_{12}$—$H_6$ (PED-6%), 363 (PED-11%)

**Table 7**
Characteristics bond critical point (BCP) of LADP.

| Atoms | Rho | DelSqRho | Ellipticity | V | G | H |
|---|---|---|---|---|---|---|
| H6 — O12 | 0.052679 | 0.140928 | 0.021851 | −0.04159 | 0.03841 | −0.00318 |
| O3 — H6 | 0.295745 | −1.61536 | 0.006549 | −0.54048 | 0.068321 | −0.47216 |
| O12 — H31 | 0.015425 | 0.042819 | 0.074265 | −0.0117 | 0.010938 | −0.00076 |
| O12 — H34 | 0.040923 | 0.118222 | 0.024193 | −0.03066 | 0.03011 | −0.00055 |
| O9 — H13 | 0.348557 | −1.99976 | 0.013772 | −0.63955 | 0.0698 | −0.56975 |
| O4 — H35 | 0.041453 | 0.119836 | 0.028175 | −0.03129 | 0.03062 | −0.00067 |
| O9 — H37 | 0.024016 | 0.069368 | 0.074627 | −0.01872 | 0.01802 | −0.00069 |
| O9 — H40 | 0.022003 | 0.062972 | 0.086651 | −0.01702 | 0.01638 | −0.00064 |

for $O_{12}$—$H_{34}$, 232(PED-19%) for $O_4$—$H_{35}$ and 523 $cm^{-1}$ (PED-10%) for $O_9$—$H_{40}$ having corresponding experimental bands in both FT-IR and FT-Raman spectrums as shown in Table 6, which confirms a shift in bands with respect to the values of electron density at the BCP.

### 3.14. Bifurcated blue and red shifting N—H···O hydrogen bonds

Hobza [76] proposed to interpret blue-shifting of hydrogen bonds by evaluating electron density transfer from LP(Y)→ σ*(XH), the proton transfer consequences, and the HX bond contraction leading to blue shifting of vibrational wavenumbers. Alabugin and Weinhold [79] interpreted the red and blue shifting hydrogen bonds in terms of hyperconjugation and rehybridization. The optimized geometry of LADP shows $NH_2^+$ group in the L-argininium cation participate in H-bond interaction and its $N_{20}$—$H_{40}$ bond is slightly shorter by 1.010 Å than other N—H bond distances (1.015 Å) and their corresponding bond lengths in XRD are 0.859 and 0.860 Å respectively, which reveals blue shifting of the hydrogen bond. In $NH_3^+$ group, N—H bond distance is $N_{17}$—$H_{34}$ for 1.053 Å, $N_{17}$—$H_{35}$ for 1.049 Å and $N_{17}$—$H_{36}$ for 1.028 Å and their corresponding bond lengths in XRD are 0.891, 0.891 and 0.890 Å respectively, which reveals that N—H···O interaction leads to elongation in the respective bond, hence red shifting H-bonds. NBO analysis predicts intermolecular hyperconjugative charge transfer energy of bifurcated hydrogen bond as 3.29 kcal/mol in $LP(O_9)\rightarrow \sigma^*(N_{20}—H_{40})$ and 3.68 kcal/mol in $LP_1(O_9)\rightarrow\sigma^*(N_{18}—H_{37})$. The decrease of $LP(O_9)\rightarrow\sigma^*(N_{20}—H_{40})$ orbital interaction energy shows the contraction of $N_{20}$—$H_{40}$ bond thereby contributing to blue shifting of the corresponding stretching wavenumber [80]. On the contrary, intermolecular hyperconjugative charge transfer energy is 7.14 kcal/mol for $LP_1(O_{12})\rightarrow\sigma^*(N_{17}—H_{34})$ and 10.63 kcal/mol for $LP_2(O_{12})\rightarrow \sigma^*(O_3—H_6)$. The increase of $LP_1(O_{12})\rightarrow\sigma^*(N_{17}—H_{34})$ and $LP_2(O_{12})\rightarrow \sigma^*(O_3—H_6)$ orbital interaction energy implies the elongation of $N_{17}$—$H_{34}$ and$O_3$-$H_6$ bonds and redshift of the corresponding stretching wavenumber. The oxygen atom in the dihydrogen phosphate anion strengthen the N—H bond in $NH_2^+$ and weakens the $NH_3^+$ groups in the L-Argininium cations.

## 4. Conclusion

The slow evaporation technique was successfully employed to grow crystal violet doped LADP crystals. The crystalline nature and lattice parameters were determined by powder X-ray diffraction technique. The twisted ICT ensuring the strong bifurcated hydrogen bond between the cations and anions charged species makes LADP to be more NLO active than other L-arginine derivatives. The vibrational spectral investigation predicts the blue shifting of N—H stretching wavenumbers in $NH_2^+$ … O and red shifting of $NH_3^+$ ….O hydrogen bonds. The NBO analysis explores the origin of blue-red shifts of bifurcated hydrogen bonds caused by hyperconjugative and electron density charge transfer interactions. In PL spectra, the luminescence broadness was found to be decreased due to dye inclusion, making the doped material better useful for blue light emitting applications with appreciable lifetime. The difference between the $\lambda_{electron}$ and $\lambda_{hole}$ suggests the LADP molecule is suitable for OLED devices. Thermal studies have demonstrated an increase in the decomposition rate with dye doping. The Z-scan technique has confirmed the enhancement of nonlinear absorption coefficient (β), third order refractive index ($n_2$), third order susceptibility ($\chi^{(3)}$) and second-order molecular hyperpolarizability (γ) in the CVLADP crystal. Theoretically and experimentally calculated field dependent second hyperpolarizability values were in agreement. Crystal violet dye incorporation was confirmed from increased transparency in the UV–visible region, band shifts in the skeletal vibrations of FT-IR and FT-Raman vibrational spectrums and enhancement of third-order NLO parameters. The bifurcated hydrogen bonded LADP molecule accomplishes high values of third-order nonlinearity and hyperpolarizability than other reported L-arginine derivatives. The suggested results show that crystal violet doped LADP crystal is more promising than pure LADP for optoelectronic and nonlinear optical devices.

## Acknowledgments

D.Sajan(D.S.) thanks to the Science Kerala State Council of Science, Technology and Environment Sasthra Bhavan, Pattom (P.O), Thiruvananthapuram – 695004, Kerala (KSCSTE), for the financial support (No. 002/SRPS/2014/CSTE dated 19-05- 2015). The authors (DS and JG) also acknowledge the DST-FIST program (SR/FST/College-182/2013, November 2013 & FIST No. 393 dated 25-09-2014) to the Bishop Moore College Mavelikara for providing the UV visible, workstation, and Photoluminescence measurements facilities. The author (DS) thank Science and Engineering Research Board, Department of Science and Technology, Government of India (DST SERB), New Delhi-110 070, for the financial support (SR/FTP/PS- 220/2012) for FT-IR measurement facilities. The author (DS) is highly grateful to Prof. T. Sundius for the Molvib program and fruitful discussions on the Normal Coordinate Analysis (NCA).

## Appendix A. Supplementary data

Supplementary data to this article can be found online at https://doi.org/10.1016/j.optmat.2019.04.019.

## References

[1] M. Mahadeva, K. Ramachandran, P. Anandan, M. Arivanandhan, G. Bhagavannarayana, Y. Hayakawa, Spectrochim. Acta, Part A 133 (2014) 396–402.
[2] Pratik M. Wankhade, Anil B. Gambhire, Gajanan G. Muley, Optik 127 (6) (2015) 3322–3328.
[3] P. Vasudevan, S. Gokul Raj, S. Sankar, Spectrochim. Acta, Part A 106 (2013) 210–215.
[4] Sahil Goel, Nidhi Sinha, Harsh Yadav, Abid Hussain, Binay Kumar, J. Mater Res. Bull. (2016) 05–023.
[5] Pascal G. Lacroix, Chem. Mater. (2001) 3495–3506.
[6] M.D. Aggarwal, J. Stephen, A.K. Batra, R.B. Lal, J. Optoelectron. Adv. Mater. (2003) 555–562.
[7] A.S. Haja Hameed, G. Ravi, R. Ilangovan, A. Nixon Azariah, P. Ramasamy, J. Cryst. Growth 890 (2002) 237–239.
[8] Kechen Wu, Caiping Liu, Chaoyong Mang, *Opt. Mater.* 29 (2007) 1129–1137.
[9] A. Joseph Arul Pragasam, S. Selvakumar, K. Thamizharasan, D. Prem Anand, P. Sagayaraj, J. Cryst. Growth 280 (2005) 271–278.

[10] Ai Qing, Peifeng Chen, Yuxiang Feng, Yebin Xu, Cryst. Growth Des. 17 (2017) 2473–2477.
[11] N. Kavitha, M. Arivanandhan, K. Ramamoorthy, K. Ragavendran, K. Sankaranarayanan, Opt. Mater. 26 (2004) 275–280.
[12] S. Arjunan, A. Bhaskaran, R. Mohan Kumar, R. Mohan, R. Jayavel, J. Alloy. Comp. 506 (2010) 784–787.
[13] G. Peramaiyan, P. Pandi, G. Bhagavannarayana, R. Mohan Kumar, Spectrochim. Acta, Part A 99 (2012) 27–32.
[14] R. Shanmugavadivu, G. Ravi, A. Nixon Azariah, A.S. Haja Hameed, T. Thenappan, Mater. Sci. Eng. B 113 (2004) 269–273.
[15] J. Zyss, T.C. Van, C. Dhenaut, I. Ledoux, *Chem. Phys.* 177 (1993) 281–296.
[16] V.S. Sukumaran, A. Ramalingam, Spectrochim. Acta 63 (2006) 673–676.
[17] M. Hirata, N. Kawasaki, T. Nakamura, K. Matsumoto, M. Kabayama, T. Tamura, S. Tanada, J. Colloid Interface Sci. 254 (2002) 17–22.
[18] Senthilkumar Chandran, Rajesh Paulraj, P. Ramasamy, Mater. Res. Bull. 68 (2015) 210–215.
[19] C.W. Tang, S.A. VanSlyke, C.H. Chen, J. Appl. Phys. 65 (1989) 3610.
[20] V.Y. Butko, X. Chi, A.P. Ramirez, Solid State Commun. 128 (2003) 431.
[21] Isabel Rozas, Ibon Alkorta, Jose Elguero, J. Phys. Chem. 102 (1998) 9925–9932.
[22] Juan Saulo González-González, Francisco J. Martínez-Martínez, Efrén V. García Baez, Alejandro Cruz, Luis Morín-Sánchez, Susana Rojas-Lima, Itzia I. Padilla-Martinez, Cryst. Growth Des. 14 (2014) 628–642.
[23] M.J. Frisch, G.W. Trucks, H.B. Schlegel, G.E. Scuseria, M.A. Robb, J.R. Cheeseman, G. Scalmani, V. Barone, B. Mennucci, G.A. Petersson, et al., Gaussian 09, Revision C.01, Gaussian Inc, Wallingford, CT, 2010.
[24] T. Sundius, J. Mol. Struct. 218 (1990) 321–326.
[25] T. Sundius, Vib. Spectrosc. 29 (2002) 89–95.
[26] E.D. Glendening, A.E. Reed, J.E. Carpenter, F. Weinhold, et al., NBO Version 3.1.TCI, University of Wisconsin, Madison, 1998.
[27] R.F.W. Bader, Atoms in Molecules, A Quantum Theory, Claderon press, Oxford, 1990.
[28] Jesby George, D. Sajan, Alex Javeesh, G. Vinitha, Dyes Pigments 165 (2019) 239–248.
[29] Jesby George, V. Sasikala, K. Lija, D. Joy, T. Sajan, P. Arumanayagam, G. Murugakoothan, Vinitha, *Opt. Mater.* 89 (2019) 48–62.
[30] Reena Ittyachan, P. Sagayaraj, Kothandapani Babu, Acta Crystallogr. E59 (2003) o886–o888.
[31] Reena Ittyachan, P. Sagayaraj, J. Cryst. Growth 243 (2002) 356–360.
[32] Rui Cheng, Junyu Ren, Jiayi Guo, Xuzhao Zhang, Shiyi Guo, J. Mater. Res. Bull. 100 (2018) 15–17.
[33] S. Yuvaraj, N. Manikandan, G. Vinitha, Opt. Mater. 73 (2017) 428–436.
[34] M. Krishnakumar, S. Karthick, K. Thirupugalmani, B. Babu, G. Vinitha, Optic Laser. Technol. 101 (2018) 91–106.
[35] Paavai Era, R.O.M.U. Jauhar, G. Vinitha, P. Murugakoothan, Optic Laser. Technol. 101 (2018) 127–137.
[36] G. Muruganandi, M. Saravanan, G. Vinitha, M.B. Jessie Raj, T.C. Sabari Girisun, Opt. Mater. 75 (2018) 612–618.
[37] R. Mohandoss, S. Dhanuskodi, G. Vinitha, Spectrochim. Acta, Part A 136 (2015) 931–936.
[38] P. Karuppasamy, Muthu Senthil Pandian, P. Ramasamy, J. Jcrysgro. 473 (2017) 39–54.
[39] M. Mahadevan, P.K. Sankar, G. Vinitha, M. Arivanandhan, K. Ramachandran, P. Anandan, Optic Laser. Technol. 92 (2017) 168–172.
[40] S. Sakthy Priya, A. Alexandar, P. Surendran, A. Lakshmanan, P. Rameshkumar, P. Sagayaraj, Opt. Mater. 66 (2017) 434–441.
[41] Jesby George, D. Sajan, Alex Javeesh, Arun Aravind, G. Vinitha, R. Chitra, Optic Laser. Technol. 105 (2018) 207–220.
[42] S. Agarwal, W. Huang, M. O'Donnell, K.C. Day, M. Day, Department of urology, University of Michigan, Ann Arbor, Michigan , N. Kotov , S. Ashkenazia 102, J. Appl. Phys. (2007) 064701.
[43] B. Kulyk, B. Sahraoui, O. Krupka, V. Kapustianyk, V. Rudyk, J. Appl. Phys. 106 (2009) 093102.
[44] A. Zawadzk, P. Płóciennik, J. Strzelecki, B. Sahraoui, Opt. Mater. 37 (2014) 327–337.
[45] K. Iliopoulos, I. Guezguez, A.P. Kerasidou, A. El-Ghayoury, D. Branzea, G. Nita, N. Avarvari, H. Belmabrouk, S. Couris, B. Sahraoui, Dyes Pigments 101 (2014) 229–233.
[46] A. Zawadzka, P. Płóciennik, Y. El Kouari, H. Bougharraf, B. Sahraoui, J. Lumin. 169 (2016) 483–491.
[47] N. Andrushchak, B. Kulyk, P. Göring, A. Andrushchak, B. Sahraoui, Acta Phys. Pol., A 133 (2018) 856–859.
[48] S. Pedro, Silva Pereira, A. Mauro, Gonçalvesa Pereira, Manuela Ramos Silva, Anna Zawadzka, Bouchta Sahraoui, José A. Paixão, Opt. Mater. 84 (2018) 606–613.
[49] M.A. Spackman, D. Jayatilaka, CrystEngComm 11 (2009) 19–32.
[50] M.A. Spackman, J.J. McKinnon, CrystEngComm 4 (2002) 378–392.
[51] L.-V. Daimay, N.B. Colthup, W.G. Fateley, J.G. Grasselli, The Handbook of Infrared and Raman Characteristic Frequencies of Organic Molecules, Academic Press, New York, 1991.
[52] D.L. Vein, N.B. Colthup, W.G. Fateley, J.G. Grasselli, The Handbook of Infrared and Raman Characteristic Frequencies of Organic Molecules, Academic Press, New York, 1991.
[53] B. Smith, Infrared Spectral Interpretation, a Systematic Approach, CRC press, Washington, DC, 1999.
[54] R.M. Silverstein, F.X. Webster, Spectroscopic Identification of Organic Compounds, sixth ed., John Wiley & Sons, New York, 2003.
[55] G. Socrates, Infrared Characteristic Group Frequencies, Wiley Interscience Publication, New York, 1980.
56 F. Arenas, I.L. Tocon, J.C. Otero, J.I. Marcos, J. Mol. Struct. 349 (1995) 29–32.
[57] R.M. Silverstein, F.X. Webster, Spectroscopic Identification of Organic Compounds, sixth ed., John Wiley & Sons, New York, 2003.
[58] T. Vijayakumar, I. Hubert Joe, C.P. Reghunadhan Nair, V.S. Jayakumar, J. Raman Spectrosc. 40 (2009) 18–30.
[59] L.J. Bellamy, The Infra-red Spectra of Complex Molecules vols. 1 and 2, Chapman & Hall, London, 1975.
[60] V. Sivasubramani, Jesby George, M. Senthil Pandian, Ramasamy Perumalsamy, K.K. Maurya, P. Pounraj, D. Sajan, New J. Chem. 42 (2018) 4261–4277.
[61] G.P. Sheeja Mol, D. Aruldhas, I. Hubert Joe, S. Balachandran, A. Ronaldo Anuf, Jesby George, Anuroopa G. Nadh, Spectrochim. Acta, Part A 212 (2019) 105–120.
[62] G.P. Sheeja Mol, D. Aruldhas, I. Hubert Joe, S. Balachandran, A. Ronaldo Anuf, Jesby George, J. Mol. Struct. 1176 (2019) 226–237.
[63] V. Alabugin, M. Manoharan, S. Peabody, F. Weinhold, J. Am. Chem. Soc. 125 (2003) 5973.
[64] Y. Wang, H. Li, S.J. Han, Chem. Phys. 123 (2005) 174501.
[65] M.E. Green, J. Phys. Chem. A 106 (2002) 11221.
[66] R.F.W. Bader, Atoms in Molecules: A Quantum Theory, Clarendon, Oxford, U.K., 1990.
[67] Yan Gao, Liqun Zhang, Yong Wang, Haoran Li, J. Phys. Chem. B 114 (2010) 2828–2833.
[68] H. Ratajczak, S. Debrus, M. May, J. Barycki, J. Baran, Bull. Polish Acad. Sci. 48 (2000) 189.
[69] M. Anis, G.G. Muley, G. Rabbani, M.D. Shirsat, S.S. Hussaini, Mater. Technol. Adv. Perform. Mater. 30 (2015) 129–133.
[70] M.S. Pandian, K. Boopathi, P. Ramasamy, G. Bhagavannarayana, Mater. Res. Bull. 47 (2012) 826–835.
[71] Chang-Guo Zhan, Jeffrey A. Nichols, David A. Dixon, J. Phys. Chem. A 107 (2003) 4184–4195.
[72] Gunasekaran Velmurugan, Balajangamanahalli K. Ramamoorthi, Ponnambalam Venuvanalingam, Phys. Chem. Chem. Phys. 16 (2014) 21157–21171.
[73] Vahram V. Ghazaryan, Boris A. Zakharov, Aram M. Petrosyana, Elena V. Boldyreva, Acta Crystallogr. C71 (2015) 415–421.
[74] G.R. Hutchison, M.A. Ratner, T.J. Marks, J. Am. Chem. Soc. 217 (2005) 2339–2350.
[75] P. Hobza, Phys. Chem. Chem. Phys. 3 (2001) 2555–2556.
[76] P. Hobza, Z. Havlas, Chem. Rev. 100 (2000) 4253–4259.
[77] P. Srinivasan, Y. Vidyalakshmi, R. Gopalakrishnan, Cryst. Growth Des. 8 (2008) 2329–2334.
[78] Alabugin, M. Manoharan, S. Peabody, F. Weinhold, J. Am. Chem. Soc. 125 (19) (2003) 5973–5987.
[79] A. LI AnYong, Sci. China Ser. B Chem. 51 (2008) 623–629.
[80] Knut R. Asmis, Nicholas L. Pivonka, Gabriele Santambrogio, Mathias Brümmer, Cristina Kaposta, Daniel M. Neumark, Ludger Wöste, Gas-phase infrared spectrum of the protonated water dimer, aff-1, Science 299 (2003) 1375–1377 http://science.sciencemag.org/content/299/5611/1375.

0925-3467
ISSN



**For Authors**

Track your accepted paper

Journal Finder

Researcher Academy

Rights and permissions

Journal Article Publishing Support Center

**For Editors**

Publishing Ethics Reso

Guest Editors